AD-A092 148 SPACE SCIENCES INC MONROVIA CALIF F/G 7/4
A MASS-SPECTROMETRIC INVESTIGATION OF CHEMICAL ASPECTS OF SEVER--ETC(U)
SEP 80 M FARBER, R D SRIVASTAVA N00014-75-C-0986
UNCLASSIFIED NL

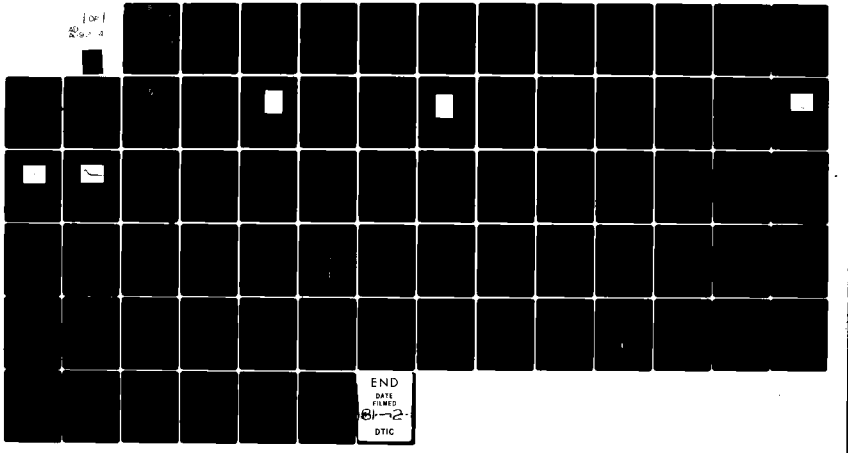

SPACE SCIENCES, INC.

135 WEST MAPLE AVENUE • MONROVIA, CALIFORNIA 91016 • [213] 357-3879

A MASS-SPECTROMETRIC INVESTIGATION OF CHEMICAL ASPECTS OF SEVERAL ENERGETIC PROPELLANTS AND EXPLOSIVES

Milton Farber and R. D. Srivastava

FINAL REPORT. 1 May 77 – 1 May 78

under

Department of the Navy
Office of Naval Research
Arlington, Virginia 22217

Contract N00014-75-C-0986

September 30, 1980

30 Sep 80

74

This research was sponsored by the Office of
Naval Research.

UNCLASSIFIED

SECURITY CLASSIFICATION OF THIS PAGE (When Data Entered)

REPORT DOCUMENTATION PAGE		READ INSTRUCTIONS BEFORE COMPLETING FORM
1. REPORT NUMBER	2. GOVT ACCESSION NO. AD-A092 148	3. RECIPIENT'S CATALOG NUMBER
4. TITLE (and Subtitle) Mass Spectrometric Investigation of Chemical Aspects of Several Energetic Propellants and Explosives		5. TYPE OF REPORT & PERIOD COVERED Final 1 May 1975 - 1 Aug 1980
		6. PERFORMING ORG. REPORT NUMBER
7. AUTHOR(s) Milton Farber R. D. Srivastava		8. CONTRACT OR GRANT NUMBER(s) N00014-75-C-0986
9. PERFORMING ORGANIZATION NAME AND ADDRESS Space Sciences, Inc. 135 W. Maple Ave. Monrovia, Ca 91016		10. PROGRAM ELEMENT, PROJECT, TASK AREA & WORK UNIT NUMBERS 122402
11. CONTROLLING OFFICE NAME AND ADDRESS Office of Naval Research 800 N. Quincy Street Arlington, Virginia 22217		12. REPORT DATE 30 September 1980
		13. NUMBER OF PAGES 72
14. MONITORING AGENCY NAME & ADDRESS(if different from Controlling Office)		15. SECURITY CLASS. (of this report) Unclassified
		15a. DECLASSIFICATION/DOWNGRADING SCHEDULE

16. DISTRIBUTION STATEMENT (of this Report)

Approved for public release; distribution unlimited.

17. DISTRIBUTION STATEMENT (of the abstract entered in Block 20, if different from Report)

18. SUPPLEMENTARY NOTES

19. KEY WORDS (Continue on reverse side if necessary and identify by block number)

Mass spectrometry	Combustion
Thermal decomposition	Plateau burning
Propellants	Super rate burning
Explosives	Lead organic salt catalysts
Ignition	Double base propellant

20. ABSTRACT (Continue on reverse side if necessary and identify by block number)

During the course of the contract chemical aspects of several propellants and explosives were investigated. Employing mass spectrometer species identification, combustion, decomposition kinetics and ignition experiments were performed to determine the mechanisms and reactions of several energetic materials. Four general categories of compounds were involved: (1) super rate and plateau burning propellants, (2) advanced gun propellant candidates, (3) the propellant and explosive compounds, 1,3,5-trinitrohexahydro-1,3,5-triazine (RDX), 1,3,5,7-tetranitro-1,3,5,7-tetraazacyclooctane (HMX),

DD FORM 1 JAN 73 1473 EDITION OF 1 NOV 65 IS OBSOLETE

UNCLASSIFIED

SECURITY CLASSIFICATION OF THIS PAGE (When Data Entered)

Block 19 - continued

Composite propellant
Electron beam deposition
Glycidyl azide polymers (GAP)
1,3,5,7-tetranitro-1,3,5,7-tetraazacyclooctane (HMX)
1,3,5-trinitrohexahydro-1,3,5-triazine (RDX)
1,3,5-triamino-2,4,6-trinitrobenzene (TATB)

Block 20 - continued

and 1,3,5-triamino-2,4,6-trinitrobenzene (TATB), and (4) a new series of high nitrogen binder materials.

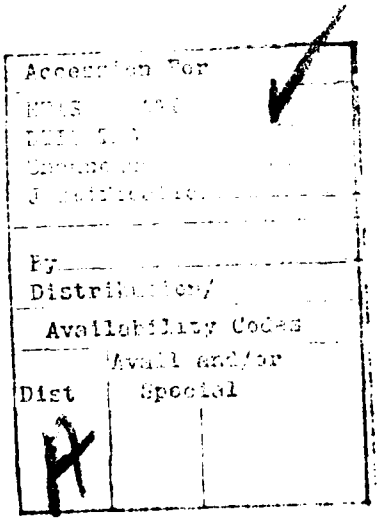

TABLE OF CONTENTS

		Page
I.	INTRODUCTION	1
II.	FIELD EMISSION ELECTRON BEAM ENERGY DEPOSITION STUDIES	3
	A. Introduction	3
	B. Theory	4
	C. Experimental Apparatus and Procedures	5
	D. Results and Discussion	14
III.	THERMAL DECOMPOSITION OF HIGH NITROGEN BINDER MATERIALS	21
IV.	PUBLICATIONS, REPORTS, AND PRESENTATIONS AT SCIENTIFIC MEETINGS	28
	A. Publications	28
	B. Reports	28
	C. Presentations	29
REFERENCES		30
APPENDIX I		
	Thermal Decomposition of 1,3,5,7-Tetranitro-1,3,5,7-Tetraazacyclooctane (HMX)	
APPENDIX II		
	Thermal Decomposition of 1,3,5-Triamino-2,4,6-Trinitrobenzene	

I. INTRODUCTION

During the course of the contract chemical aspects of several propellants and explosives were investigated. Employing mass spectrometer species identification, combustion, decomposition kinetics and ignition experiments were performed to determine the mechanisms and reactions of several energetic materials. Four general categories of compounds were involved: (1) super rate and plateau burning propellants, (2) advanced gun propellant candidates, (3) the propellant and explosive compounds, 1,3,5-trinitrohexahydro-1,3,5-triazine (RDX), 1,3,5,7-tetranitro-1,3,5,7-tetraazacyclooctane (HMX), and 1,3,5-triamino-2,4,6-trinitrobenzene (TATB), and (4) a new series of high nitrogen binder materials.

The ignition and combustion mechanisms of the plateau burning propellants containing lead and copper salt additives, including N-5 and HEX-12, were investigated. These were double base, nitroglycerine nitrocellulose propellants with approximately 2.5 to 5% lead additives. A mass spectrometric analysis of the thermal decomposition of several metallic organic additives, including acetates, salicylates and resorcylates of lead, copper, silver and manganese was completed. The results of this work have been previously reported, noted in Section IV. as A.1, B.1, and C.1.

Following the plateau burning propellant investigations, studies of minimum smoke composite and double base propellants containing lead oxide and carbon black as catalytic ingredients were undertaken. Included were ammonium perchlorate and HMX composities, designated as N1010, N1013 and N1016, prepared at Thiokol's Wasatch Division,

and a double base formulation, FZO, from Allegany Ballistics Laboratory. The thermal decomposition of RDX was also determined. Results of these studies were reported earlier, listed in Section IV. as A.2, B.2, and C.1.

The third phase of the program included investigation of advanced catalytic double base formulation gun propellants from the Naval Ordnance Station, Indian Head. Mass spectrometric experiments were conducted on propellant ignition products and thermal decomposition of the catalytic lead chelates of benzophenone, alizarin, and chrysazin. Also included in this phase of studies was the determination of the sublimation and thermal decomposition of HMX and TATB. The results of this phase have been presented previously, listed in Section IV. as B.3, C.3 and C.4.

The concluding phase of the program during the past year involved (1) completion of the sublimation and thermal decomposition of HMX, (2) TATB studies by Langmuir and Knudsen effusion mass spectrometry, (3) a study of the effects of high energy deposition in fast times on HMX employing a field emission electron beam apparatus designed and constructed by scientists at this laboratory, and (4) the commencement of investigation of the thermal decomposition of a new series of high nitrogen binder materials synthesized at various laboratories. The high nitrogen binder materials include glycidyl azide polymers (GAP), and 3,3bis(azidomethyl)oxetane (BAMO). Preliminary mass spectrometric thermal decomposition results of GAP are presented in Section III.

The following sections of this report include discussions of the field emission electron beam energy deposition system, the results of fast time high energy depositions on HMX, and the thermal decomposition of high nitrogen binder materials, as well as a list of publications, reports, and presentations at scientific meetings. Details of the HMX and TATB studies are presented in Appendix I and Appendix II, respectively, which are preprints of articles in the process of publication.

II. FIELD EMISSION ELECTRON BEAM ENERGY DEPOSITION STUDIES

A. Introduction

In order to deposit a higher energy than that obtainable by conventional heating a field emission electron beam (E-beam) system was designed and constructed at this laboratory.[1-3] This apparatus allows energy depositions of as much as 2 joules at 100,000 volts in short times on the order of 60 to 100 nanoseconds. When the maximum energy deposition obtained from 100 keV electrons is employed, temperatures as high as 20,000 K and pressures of over 300 atmospheres are produced. The vapor released upon deposition of the E-beam energy arrives at the source of a quadrupole mass spectrometer in a few microseconds. In these short times any vapor originating from the sample does not have sufficient time for recombination and thus mass spectrometer identification indicates the species leaving the target surface. The relatively low voltages of 50 to 100 kV allows the electrons to only penetrate the sample area a very short distance,[4] 0.01 - 0.1 mm, thereby creating conditions for maximum

vaporization. The shallow penetration of the electrons produces vapor species similar to those from high power pulsed lasers.[1]

After assembly of the complete system, E-beam deposition experiments were performed on HMX samples. The following sections describe the theory, apparatus, and results obtained.

B. Theory

The energy deposited in a short interval of time must theoretically equal the energy absorbed in various components as a result of this deposition.

$$E_{deposited} = \int C_p dT + KE_{blow\text{-}off\ material} + h\nu_{(radiation)} \qquad (1)$$

where

$E_{deposited}$ = the total energy delivered by the E-beam pulse unit to the target;

$\int C_p dT$ is the enthalpy rise in the target;

$KE_{blow\text{-}off\ material}$ is the energy received by both the vapor species and the solid or liquid blow-off material; and

$h\nu_{(radiation)}$ is the energy lost due to radiation.

Likewise, momentum must be conserved, and therefore the impulse accorded to the target equals the summation of the impulse blow-off materials:

$$I = \sum m_g v_g + \sum m_s v_s \qquad (2)$$

where

I = total impulse received by the target;

$\sum m_g v_g$ = sum of momentum of all gaseous species; and

$\sum m_s v_s$ = momentum of solid or liquid spall.

The obtaining of experimental data for the various components including (1) E, the total energy deposited, (2) I, the impulse, (3), m, the total mass loss, (4) m_g, the composition of the vapor including neutral and ionic species, (5) $\int C_p dT$, the enthalpy rise in the sample, (6) v_g, the velocity of the gaseous and ionic species, and (7) $h\upsilon$, the radiation lost during the pulse will allow the solution of the energy and impulse equations.

C. Experimental Apparatus and Procedures

The experimental apparatus consists of several primary units including a pulse unit, a field emitting source, a vacuum electrobalance, photo cell radiation detectors, sample enthalpy measuring unit, and a quadrupole mass spectrometer. Figure 1 is a schematic diagram showing the complete assembly of this apparatus. Figure 2 is a cut-away diagram of the vacuum chamber in which the various components are shown. A brief description of the components is presented below.

1. Pulse Unit

The pulser (Femco Model 730-231) is based on the Cockroft-Walton technique in which an array of capacitors (plus pulse shaping inductors) is charged in parallel and then discharged in series, through spark gaps, to give an output voltage pulse which is a multiple of the charging voltage. This pulser is designed to be charged

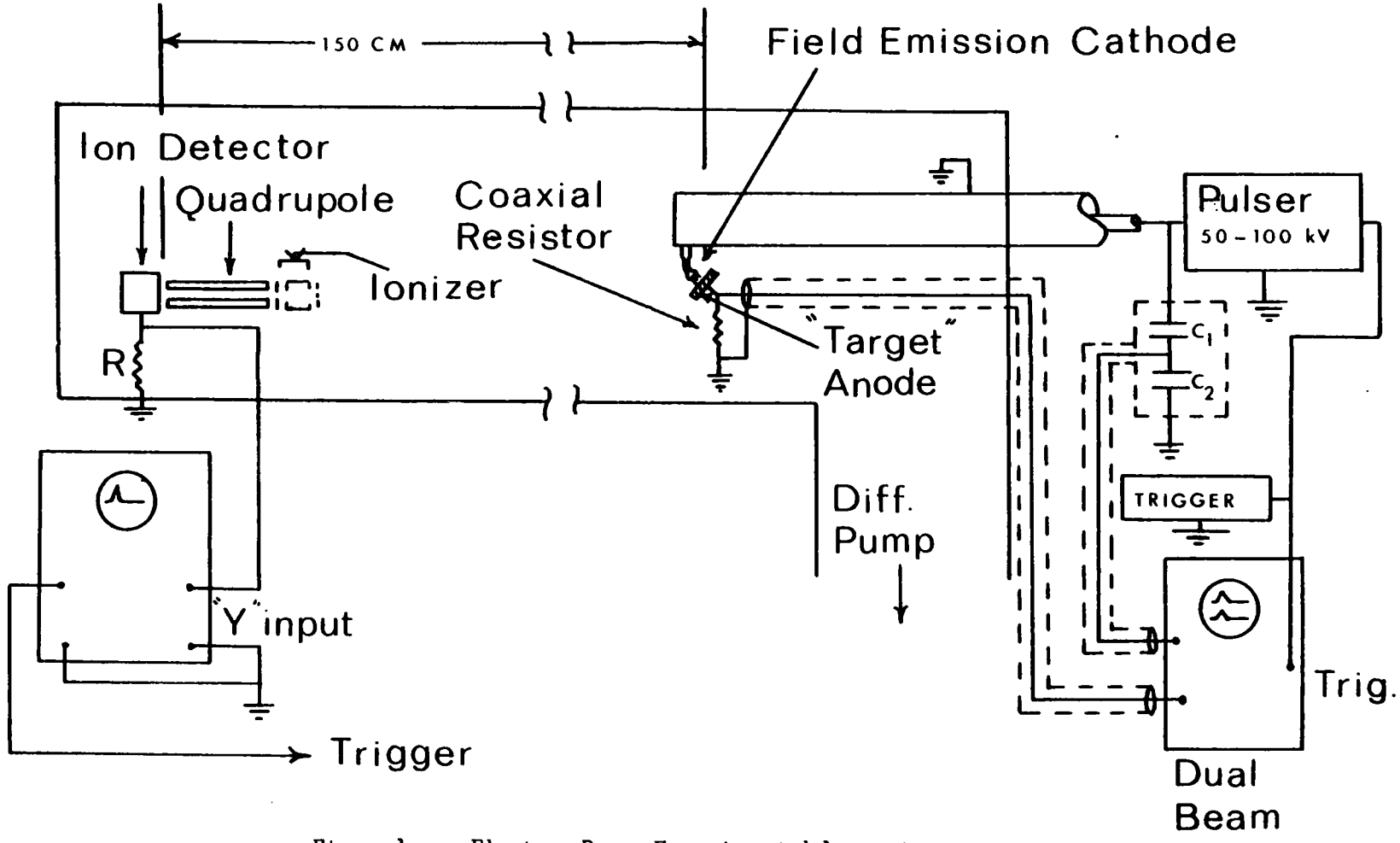

Figure 1. Electron Beam Experimental Apparatus

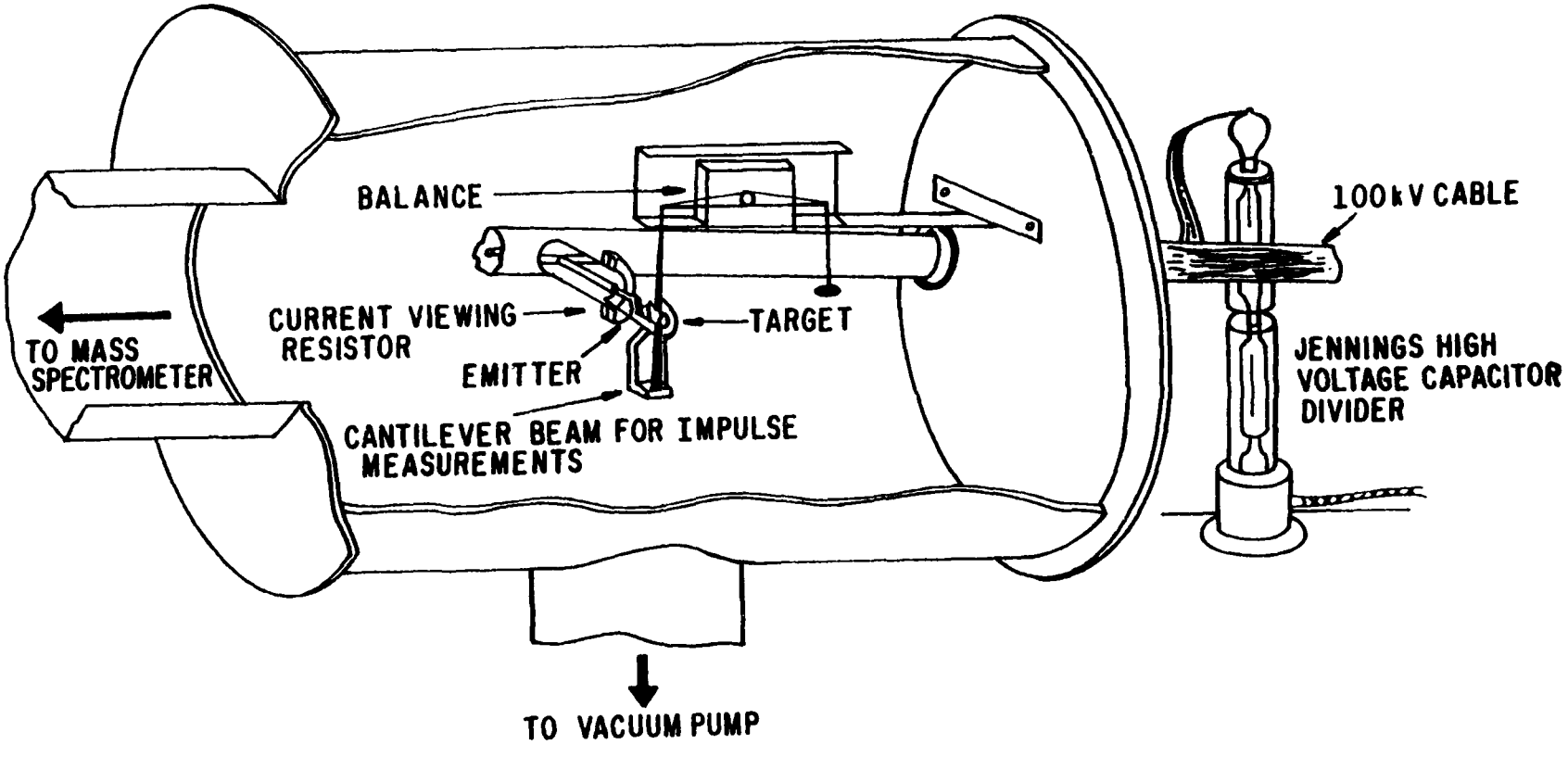

Figure 2. Vacuum Chamber Showing Field Emitting Cathode and Target

to 30 kV and to deliver 105 kV peak voltage when discharged into a 75 ohm coaxial cable correctly terminated. The discharge is initiated by a high voltage pulse applied to a triggered spark gap. The range of charging voltage is determined by pressurizing the spark gap chamber with dry nitrogen. In order to protect the pulser from reflected voltage pulses the coaxial cable is terminated with a spark gap in parallel with the emitter.

The pulse current is measured with a coaxial resistor. The current viewing resistor is connected directly to the vertical diffraction plates of an oscilloscope. The impedance of this resistor is approximately 0.043 ohms and the vertical deflection sensitivity of the oscilloscope is 50 V/cm. The voltage traces are made employing a Jennings capacitor network consisting of a high voltage vacuum divider and a vacuum capacitor supplying a voltage division of 675/1.

2. Field Emitting Source

The field emission arrays are patterned after the field emitters of W. P. Dyke (U. S. Patent 3,283,203). These devices contain arrays of microscopic field emitting points and produce electron beams directly onto an external target. The field emitters employed are arrays of short molybdenum wires, 0.05 mm dia. (.002" dia.) electropolished in sodium hydroxide solution to form points with diameters of .01 mm or less. The mounting of the field emitting cathode and target are shown schematically in Figs. 1 and 2. The probe is placed such that the target surface is on the axis of the mass spectrometer (horizontal) and on the axis of the vertical port which is used for the

mass-loss balance. The coaxial probe consists of an outer conducting tube of 1 1/4" dia. and an inner conducter of 3/8" dia. The side tube is 7/8" dia. with and inner conducter of 1/4" dia. These dimensions (with vacuum insulation) correspond closely with a characteristic impedance of 75 ohms, the impedance of the high voltage pulser and cable. The spacing of inner and outer conducters is maintained by glass insulators designed to resist flash-over.

The spacing of the emitter in relation to the target is governed by space charge limitations, system impedance, and beam energy components. Since the impedance of the pulser and the impedance of the transmission cables is 75 ohms, it is necessary to provide a field emitter impedance of 75 ohms to obtain maximum deposition of the pulse energy. The field emission across the discharge is controlled by the electron distribution through a plasma as given by the equation

$$I = \frac{2.33 \times 10^{-6} \times A \times V^{3/2}}{d^2} \tag{3}$$

from which the impedance, Z, can be calculated

$$Z = \frac{V}{I} = \frac{d^2}{2.33 \times 10^{-6} \times A \times V^{1/2}} \tag{4}$$

where I is current in amperes/mm^2; V is voltage in volts; Z is impedance in ohms; d is spacing between needles and sample, mm; and A is target area, mm^2. This allows a fairly accurate calculation of the spacing of the needle area and target to obtain a matched impedance. The

field emission area is approximately 2 square millimeters and the distance from the target is slightly under 1 millimeter.

3. Mass Measurements

A Cahn electro microbalance is employed for the measurement of the mass losses. This balance, having a sensitivity of .05 micrograms, is installed as an integral part of the apparatus in the high vacuum enclosure. A schematic is presented in Fig. 3.

Changes in sample weight cause the beam to deflect, momentarily. This motion changes the ph tube current, which is amplified and applied to the coil attached to the beam. The coil is in a magnetic field, so current through it exerts a moment on the beam, restoring it to balance. The coil current is thus a measurement of sample weight, in accordance with Ampere's Law. The self-centering elastic ribbon suspension eliminates friction, and defines the axis of rotation. Variations in ribbon rotational stiffness as a result of temperature and age, and hysteresis do not affect balance readings as they would in torsion-type balances, due to the very small angle of rotation, and since readings are always made at the same angular position.

The symmetrical beam construction permits taring of heavy containers, or the fixed part of the sample weight, by counterposing on loop C. This permits finer precision as a fraction of total load than would be possible with electrical taring only, down to finer than one part per million. Use of a phototube to detect beam position ensures that the detector cannot exert any force on the beam.

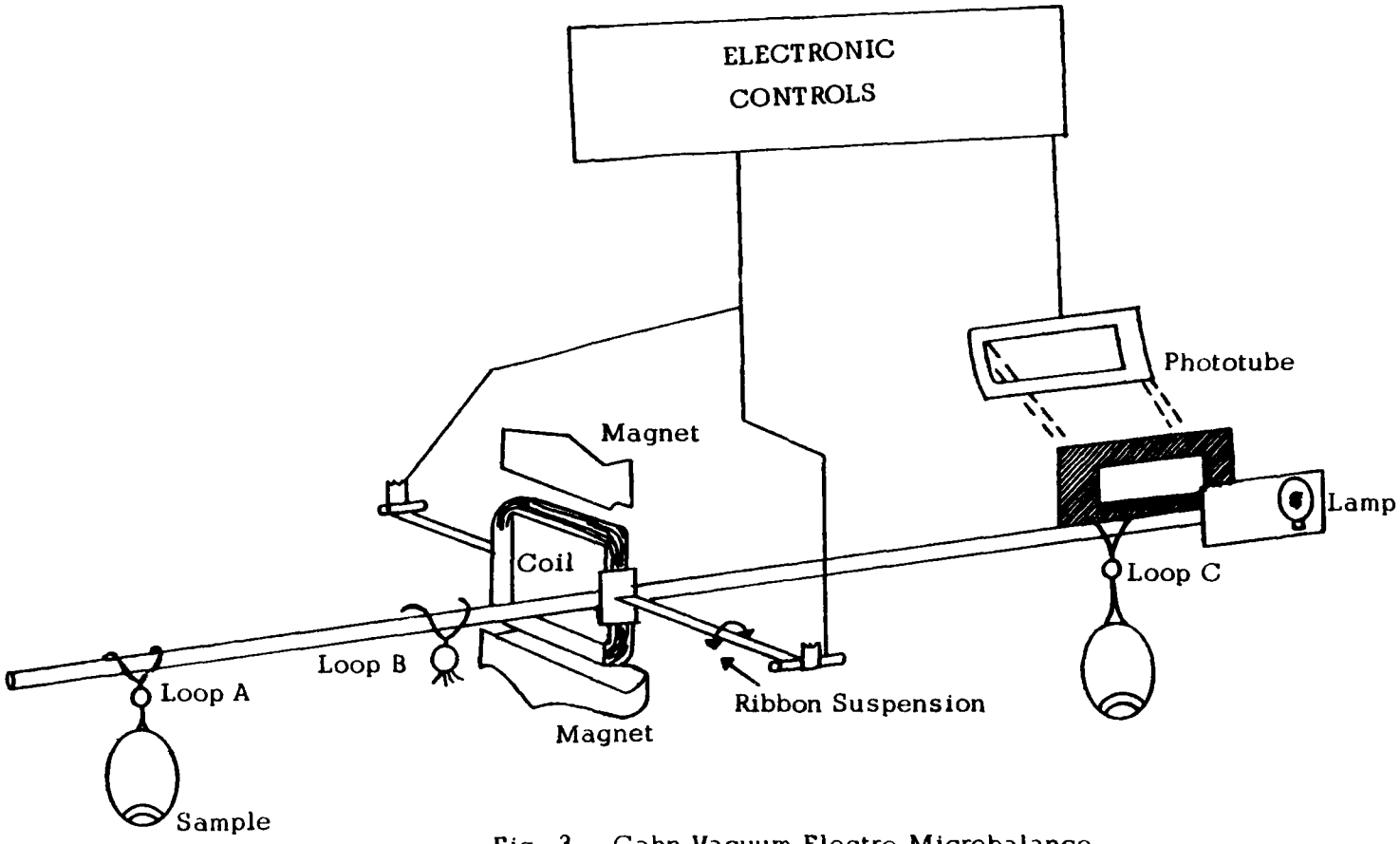

Fig. 3. Cahn Vacuum Electro Microbalance

The electrobalance does not require any kind of "gain" or "damping" control. The same high-gain feedback system also speeds up balance response many fold over what it would be without the feedback.

4. Enthalpy Rise

The heat rise in the target sample is measured by a sensitive iron-constantan thermocouple array located inside the body of the target. The sensitivity for a six-thermocouple array is 0.001 C. The background pressure in the vacuum chamber during all the experiments is 10^{-5} torr.

5. Radiation Effect

Although the energy released as radiation is small compared to the total energy released (less than 1%), the radiation measurement may be an indication of "first light" of propellant or explosive decomposition. A photomultiplier and blue and red photocells are used for the determination of the radiation released during an E-beam deposition. The blue and red cell responses as shown in Fig. 4 correspond to only 10^{-8} joules of energy, which is negligible to the total energy released.

6. Quadrupole Mass Spectrometer

The mass species, both ionic and molecular, resulting from blow-off are quantitatively identified by means of a quadrupole mass spectrometer attached to the vacuum chamber at distances of 30 and 100 cm from the target. The mass spectrometer has a resolution of 500 and a sensitivity of 10^{-14} torr for N_2 when an electron multiplier is used in conjunction with an electrometer

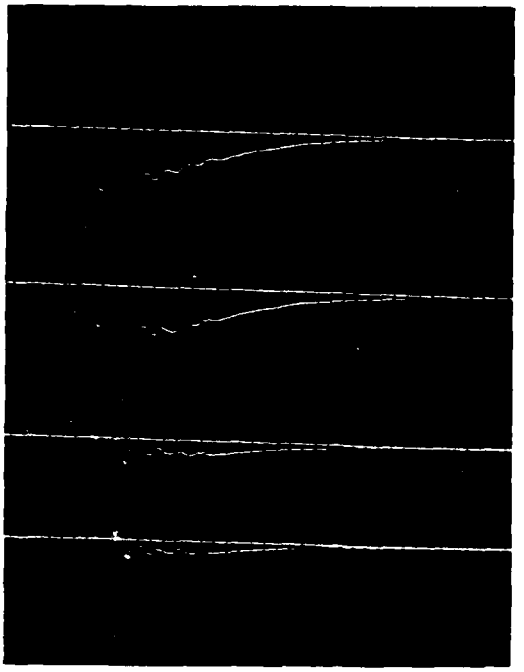

Fig. 4. S4 and S1 Photocell Response

amplifier.[5] The quadrupole probe, mounted on a 4" Ultek flange, is a compact unit which can be inserted 9" into the vacuum chamber (Figs. 1 and 2).

The quadrupole mass filter accepts a much wider distribution of transverse velocities than does the time-of-flight, for similar resolution. Photons, neutral species, and ions will be detected by the electron multiplier. Photons and neutral molecules will pass through the quadrupole if they possess sufficient energy and enter parallel to the poles. The time and point of injection, and the direction and magnitude of the initial velocity will have no important effect on the resolution of the quadrupole mass filter. The instrument is insensitive to RF radiation and other electrical noises. As a precautionary measure, the radiation of RF into the room is eliminated by the use of a grounded shield completely surrounding the electronic equipment which is used to generate the high voltage electron emission. Ground loop currents are also eliminated such that a few ions per second arriving at the electron multiplier can be detected.

D. RESULTS AND DISCUSSION

1. E-Beam Parameters and Diagnostics

Energy deposition in the megawatt range were made on the sample target in times of less than 100 nanoseconds. A typical E-beam diagnostic is shown in Fig. 5. The profiles of the voltage, current and power are shown graphically, as reproduced from the actual oscilloscope tracings, as shown in Fig. 6. Figure 7 depicts the energy deposited as a function of the input voltage from 50 to 100 kV.

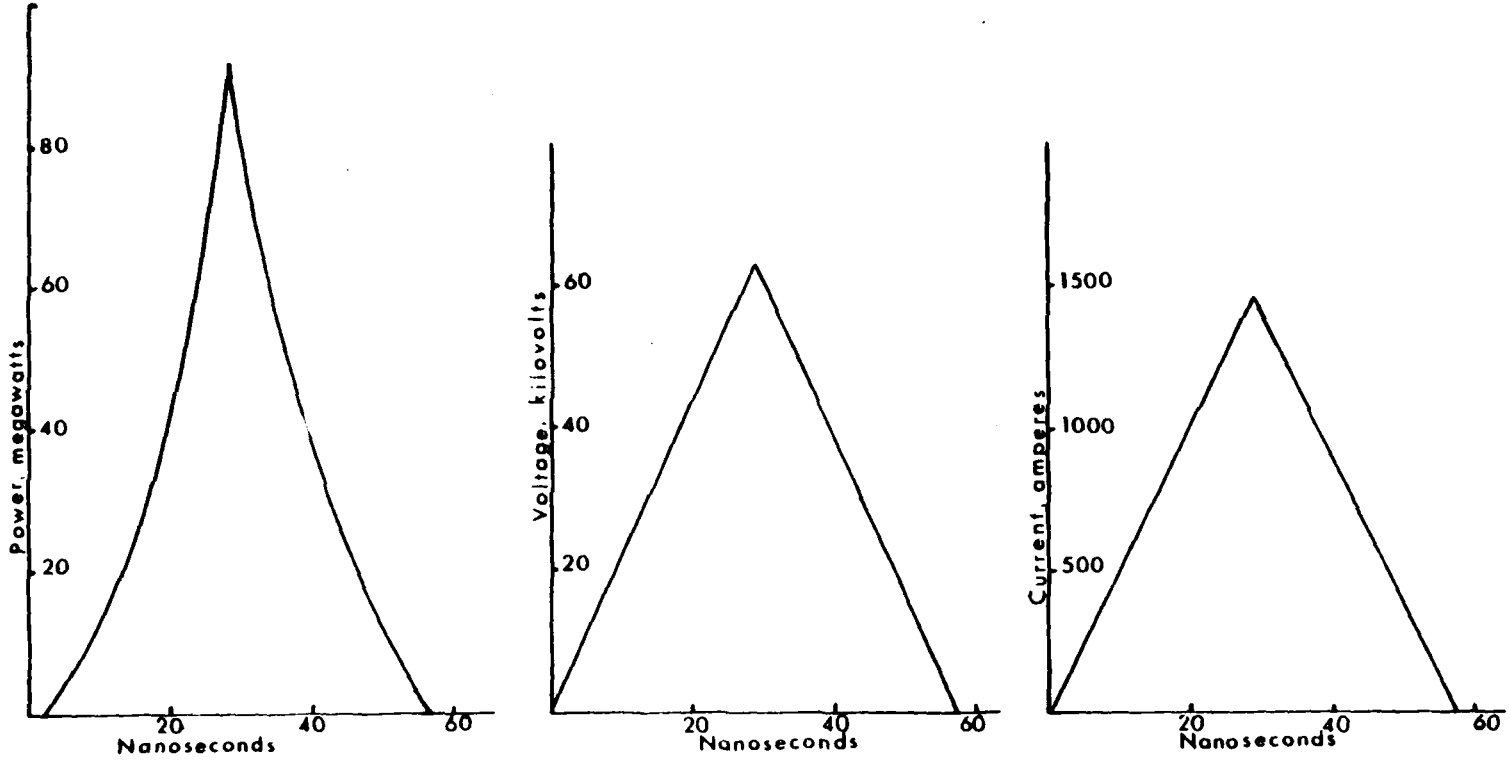

Fig. 5. E-Beam Diagnostics at a Charging Voltage of 100 kV)
Pulse length = 57.6 nanoseconds
Average power = 30.9 megawatts
Peak power = 92.0 megawatts
Energy deposited = 1.78 joules

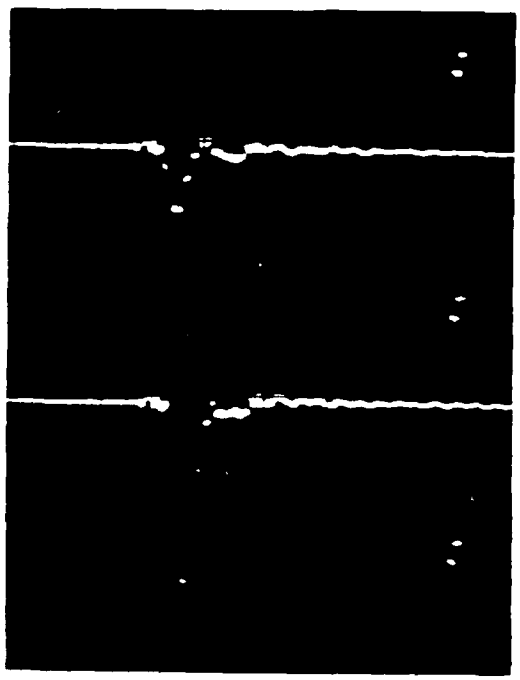

Current
145.6 amperes/mm
22.2×10^{-9} sec/mm

Voltage
3760 volts/mm
22.2×10^{-9} sec/mm

Fig. 6. Current-Time and Voltage-Time for 100 kV Charging Voltage (Dummy Load)

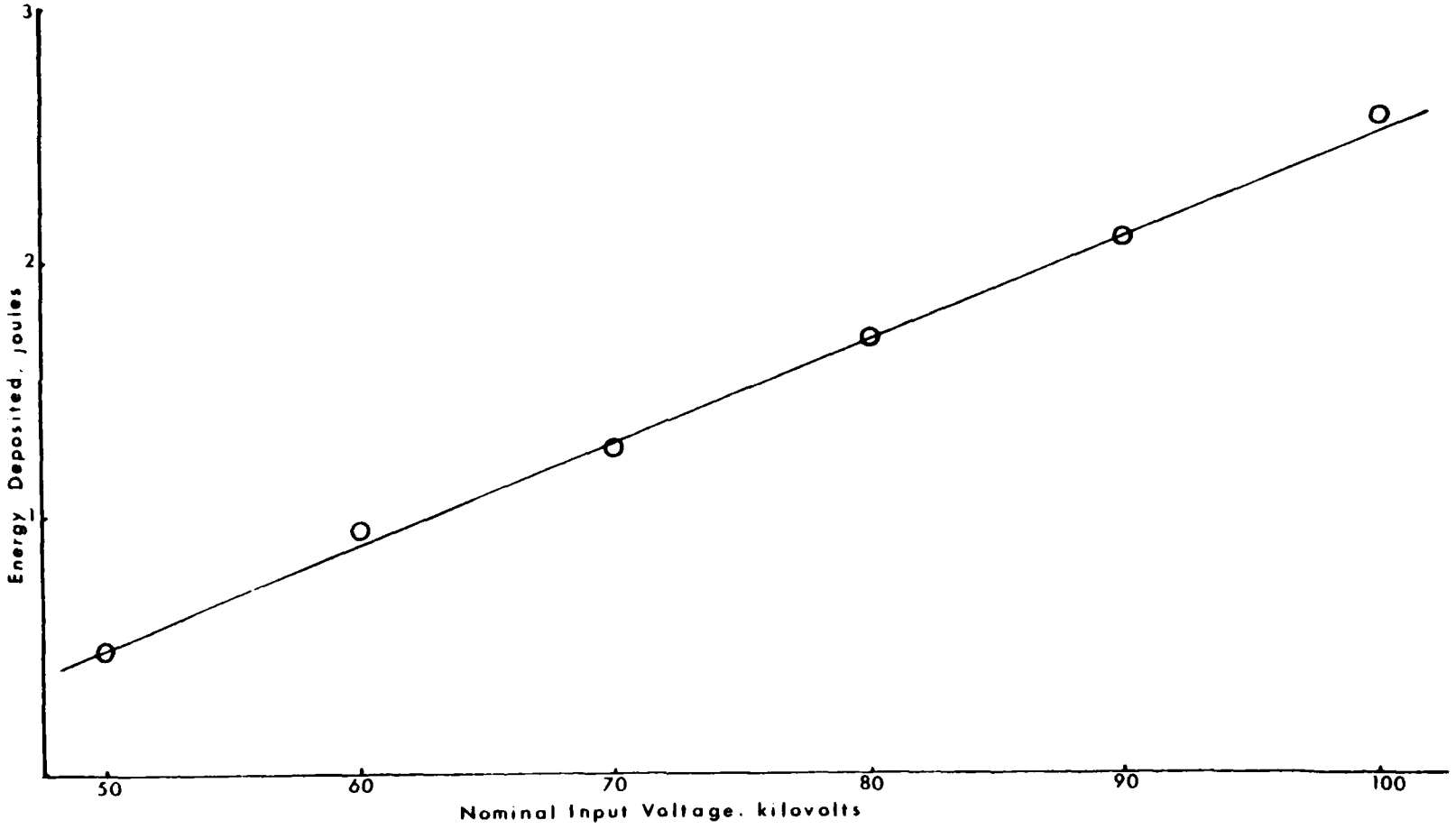

Fig. 7. Energy Deposited vs. Nominal Input Voltage for Aluminum

The actual penetration of 50 to 100 keV electrons is very small. According to Spencer,[4] million-volt electrons will penetrate carbon samples to depths of a centimeter or more, whereas 50 to 100 keV electrons can only penetrate a target a fraction of a centimeter. For example, a 50 keV electron will penetrate a carbon target to a depth of 2.2×10^{-2} mm. Thus the adsorption of the electrons on the top layers of the target produce very high temperatures and pressures. On the surface, initial temperatures and pressures as high as 20,000 K and 300 atmospheres are produced. At a distance of 1 mm from the surface the pressure is 20 atmospheres, which rapidly decays to 10^{-6} atmospheres at a distance of 1 meter from the surface. The resultant vapor species are kinetic and not in thermodynamic equilibrium. Figure 8 shows the vapor species produced from E-beam depositions on amorphous carbon. At the lower fluences the concentration of the species tends toward the equilibrium values.

A number of experimental checks were made to determine the validity of the technique. These included: (1) radiative and atomic recombination, and (2) the effects of the electric field, the magnetic field and hydrodynamics on the species and ion velocities. These have been discussed in detail previously.[1,3] These experiments established that the species, as determined mass spectrometrically, were those produced from E-beam energy deposition, and not from recombinations of atomic and molecular species in the plasma.

2. E-Beam Depositions on HMX

The sublimation and vacuum thermal decomposition studies on HMX have been completed (see Appendix I) and a

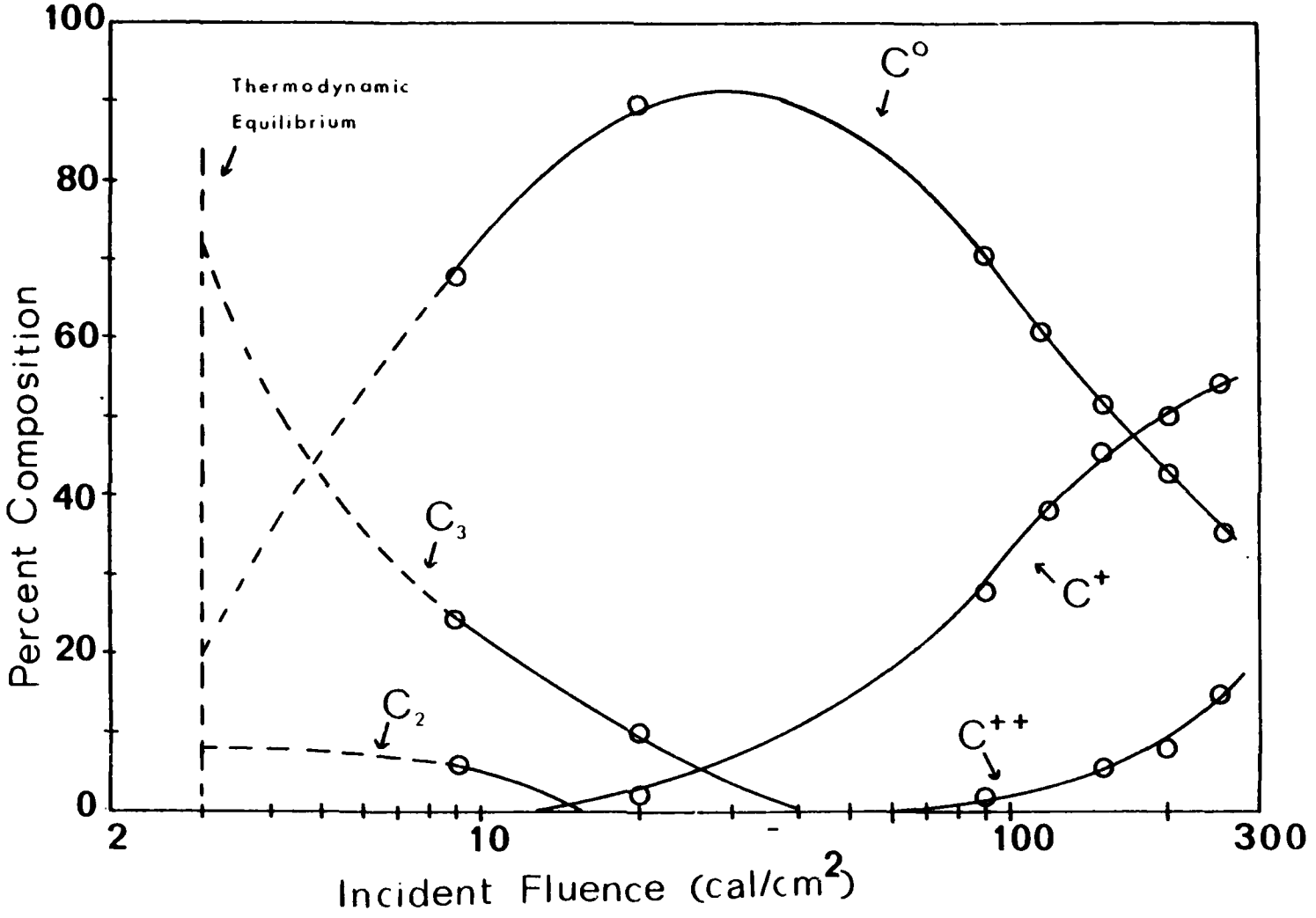

Figure 8. Concentration of Species vs. Incident Fluence for Amorphous Carbon

decomposition mechanism involving the ring cleavage of HMX into two equal fragments

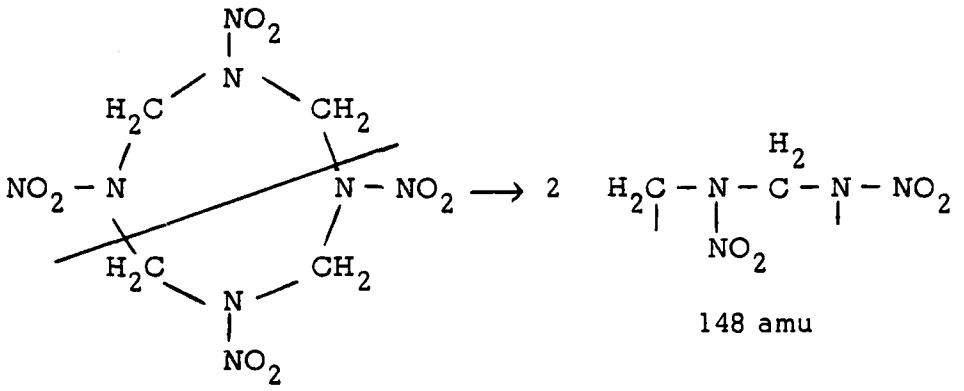

296 amu

148 amu

as the primary mode of thermal decomposition has been derived. The 148 amu fragments undergo further decomposition to numerous small fragments.

In order to determine the molecular decomposition at high energy depositions in fast times, HMX samples were investigated in the E-beam apparatus. The sample, which weighed approximately 5 mg, was placed in a hole approximately 10 square mm in area and 1 mm deep drilled in a 1 square cm carbon block. The E-beam was operated at a voltage of 50 keV. The beam deposition time was approximately 0.1 microseconds. An electron beam current of over 1000 amperes deposited 0.5 joules of energy on the HMX sample. Thus the entire 0.5 joules of energy were deposited on a very small

mass of HMX, producing a high temperature and a considerable quantity of vapor species.

The electrons arrive at the mass spectrometer (a distance of 30 cm) within a microsecond after the E-beam pulse. The horizontal scale in Fig. 9 is 1 μsec/cm and shows the decay curve of the electrons reaching the mass spectrometer. Figure 10 depicts the amu 148 peak arriving at the mass spectrometer 40 microseconds after pulse. The vertical scale is 20 mv/div as compared to 1000 mv/div for the scale in Fig. 9.

The HMX molecules can also be seen at amu 296 in Fig. 11. In addition to the 148 and 296 amu peaks, numerous smaller peaks were apparent, as well as ionic species. When the ionization chamber of the mass spectrometer is turned off the ions produced are observed. The E-beam results support the data obtained in the vacuum decomposition studies.

III. THERMAL DECOMPOSITION OF HIGH NITROGEN BINDER MATERIALS

Recent synthesis efforts have been successful in producing energetic binding materials containing a high percentage of nitrogen. Azide groups have been used in glycerine type molecules to form fairly stable polymeric species. Several of these compounds and polymers, synthesized at various laboratories, containing single and double azide groups have been received. The first to be investigated was a sample of glycidyl azide polymer, GAP,

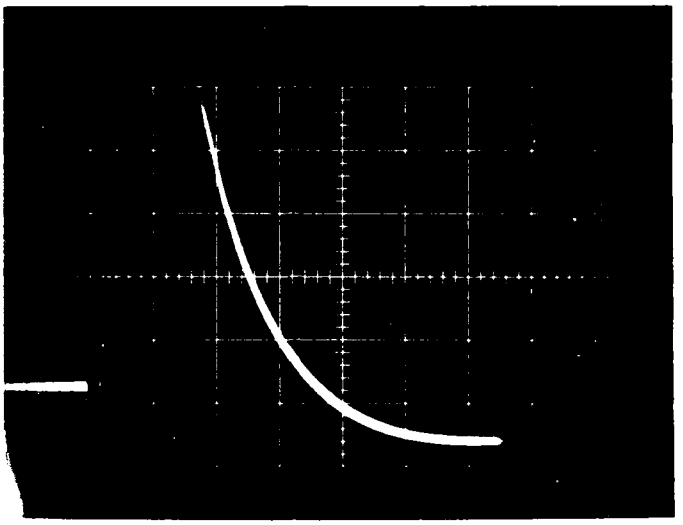

Fig. 9. Intensity-time photograph of 50 keV E-beam deposition.

Initial electron cloud from E-beam arriving at the mass spectrometer within 1 μsec.

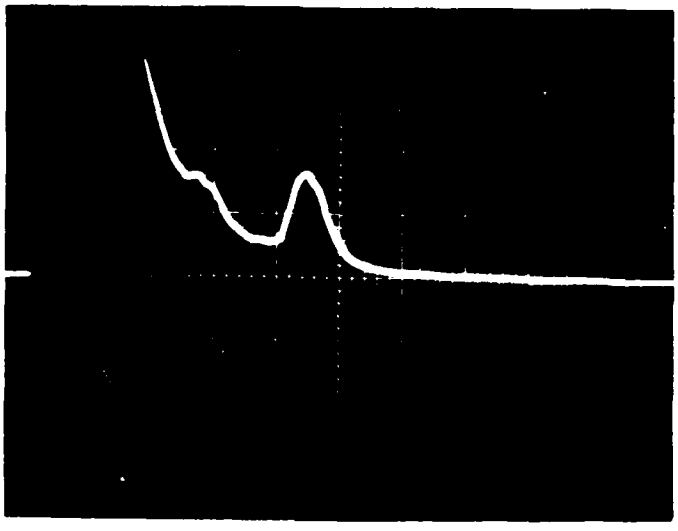

Fig. 10. Intensity-time photograph of 50 keV E-beam deposition.
The amu 148 decomposition fragment arriving at the mass spectrometer within 40 μsec after E-beam deposition.

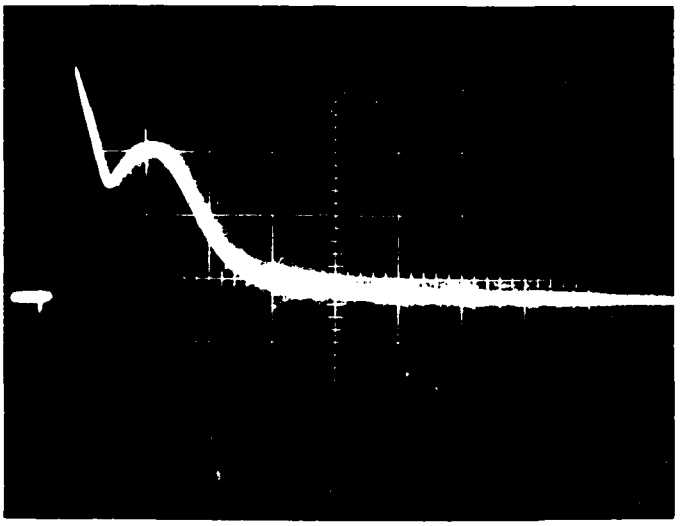

Fig. 11. Intensity-time photograph of 50 keV E-beam deposition on HMX. The 296 (HMX) molecule arrives at the mass spectrometer within 50 μsec after E-beam deposition.

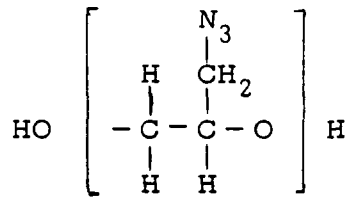

Preliminary thermal decomposition studies on GAP were commenced employing the dual vacuum mass spectrometer system. Initial experiments were performed to determine the manner of polymer decomposition. The first species to arrive at the mass spectrometer upon heating the sample was molecular nitrogen, indicating that the azide group is the first to decompose. Figure 12 shows the relative intensities of N_2 as a function of the effusion cell temperature. At approximately 120 C GAP begins to lose N_2 and the rate of evolution increases with temperature.

A secondary phase of decomposition, the breaking of the organic backbone, takes place at approximately 170 C, with the release of an amu 30 species. Figure 13 shows the mass spectra of this phase of the decomposition. The 30 amu molecule may be formaldehyde, H_2CO, appearing from the fracturing of the glycidyl chain of the GAP molecule. The temperatures given in Fig. 12 and Fig. 13 are those of the cell and should be considered as approximate. Future experiments will entail more precise temperature measurements with thermocouples imbedded within the polymer as well as in the wall of the cell. From the decomposition products observed it is expected that a thermal decomposition mechanism and an energy of activation value can be derived.

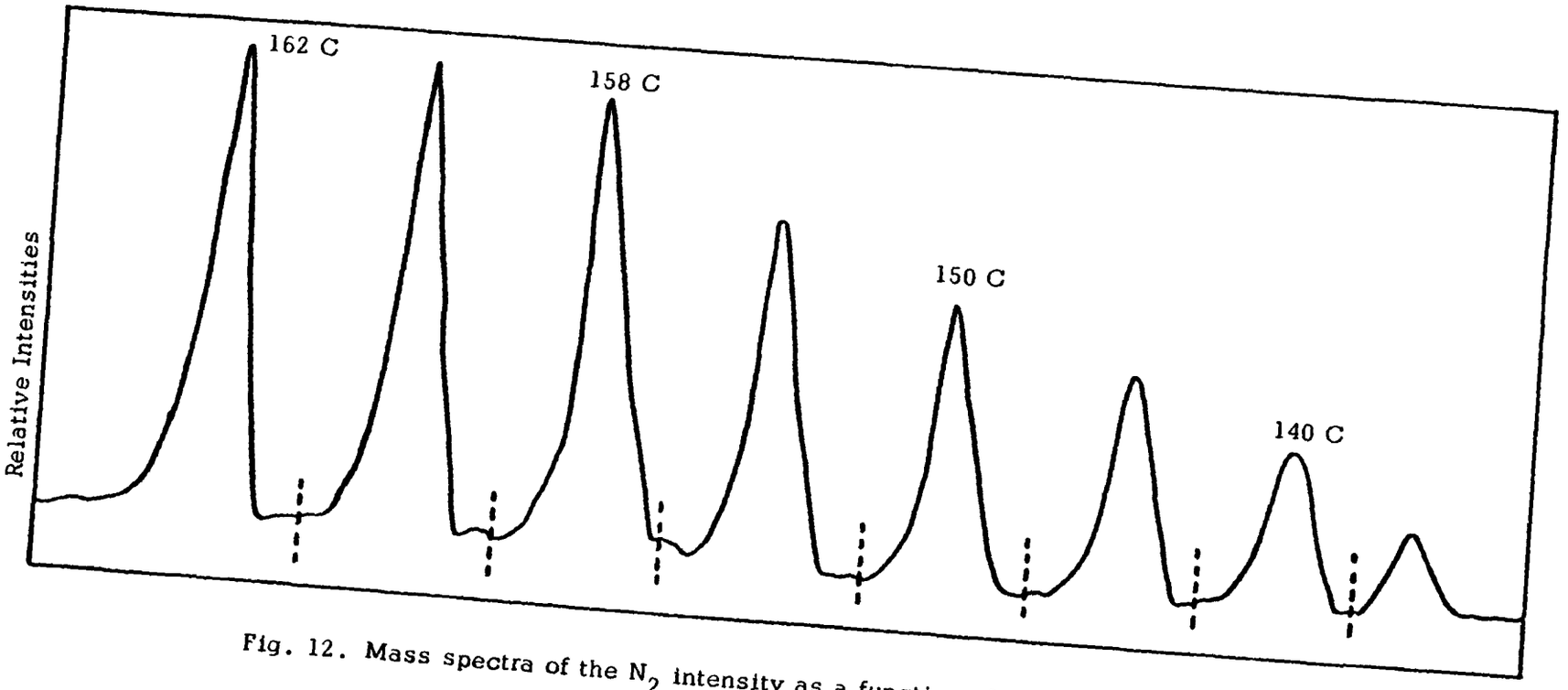

Fig. 12. Mass spectra of the N_2 intensity as a function of temperature from the thermal decomposition of GAP, glycidyl azide polymer.

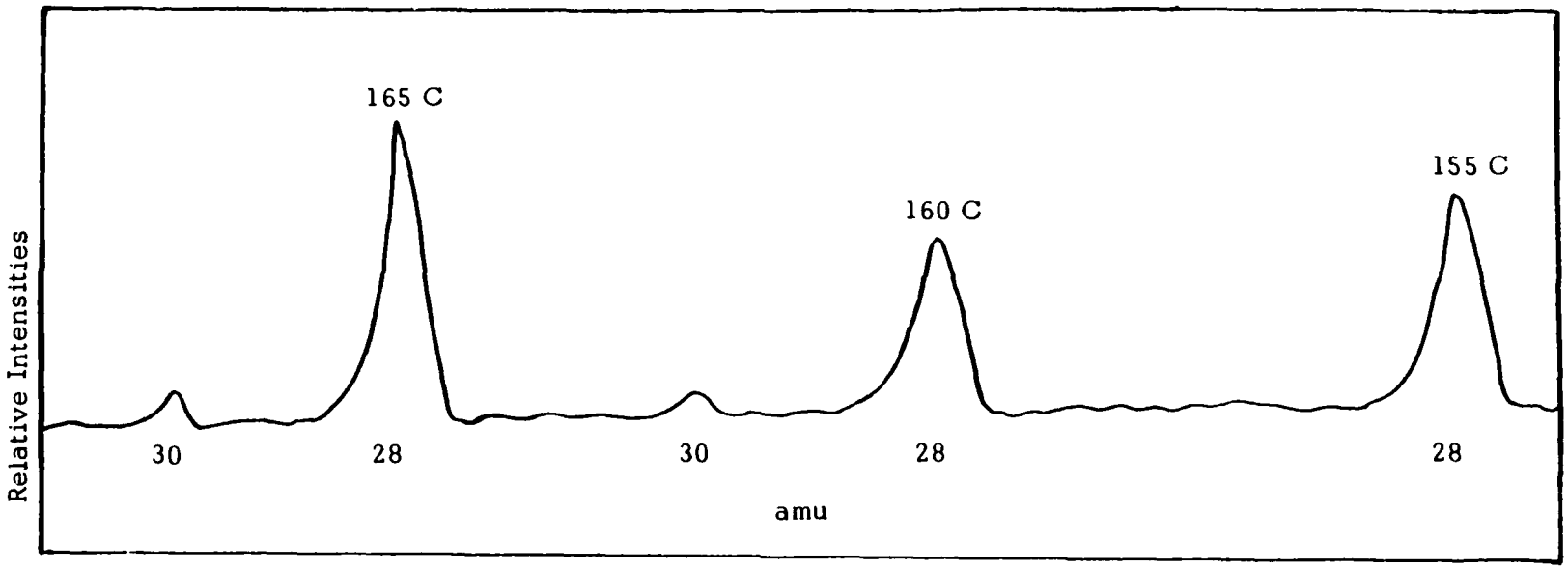

Fig. 13. The appearance of the 30 amu species, possibly formaldehyde, H_2CO, from the secondary decomposition of GAP, indicating a breakdown of the organic backbone of the polymer.

IV. PUBLICATIONS, REPORTS, AND PRESENTATIONS AT SCIENTIFIC MEETINGS

A. Publications

1. M. Farber and R. D. Srivastava, "A Mass-Spectrometric Investigation of the Chemistry of Plateau Burning Propellants," Combustion & Flame," 31, 309 (1978).

2. M. Farber and R. D. Srivastava, "Mass Spectrometric Investigation of the Thermal Decomposition of RDX," Chem. Phys. Lett. 64, 307 (1979).

3. M. Farber and R. D. Srivastava, "Thermal Decomposition of 1,3,5,7-Tetranitro-1,3,5,7-Tetraazacyclooctane (HMX)," in process of publication (1980), see Appendix I.

4. M. Farber and R. D. Srivastava, "Thermal Decomposition of 1,3,5-Triamino-2,4,6-Trinitrobenzene," in process of publication (1980), see Appendix II.

B. Reports

Technical Report No. 1, "A Mass Spectrometer Investigation of the Chemistry of Plateau Burning Propellants," November, 1976.

2. Annual Summary Report, "A Mass Spectrometric Investigation of the Chemistry of Advanced Composite and Double Base Propellants," August, 1978.

3. Annual Summary Report, "A Mass Spectrometric Investigation of the Decomposition Products of Advanced Propellants and Explosives," August, 1979.

C. Presentations

1. 15th JANNAF Combustion Meeting, September 11-15 1978, Naval Underwater Systems Center, Newport, Rhode Island.

2. 16th JANNAF Combustion Meeting, September 10-14 1979, Naval Postgraduate School, Monterey, California.

3. Conference on Thermal Decomposition of Propellants and Explosives, U. S. Air Force Academy, Colorado, 2-3 August 1979.

4. JANNAF Propulsion Systems Hazards Workshop, 15-16 April 1980, Eglin Air Force Base, Florida.

REFERENCES

1. M. Farber, J. E. Robin and R. D. Srivastava, J. Appl. Phys. 43, 3313 (1972).
2. M. Farber, Technical Report No. AFWL-TR-70-49, "Experimental Determination of Energy of Sublimation and Blow-Off Impulse," November 1970.
3. M. Farber, J. E. Robin and R. D. Srivastava, Technical Report No. AFWL-TR-71-92, "Experimental Determination of Energy of Sublimation for Amorphous Carbon, Phenolic Resin, Carbon Phenolic and Fused Cast Silica," March 1972.
4. L. V. Spencer, "Energy Dissipation by Fast Electrons," Natl. Bur. Stds. (U.S.) Monograph No. 1, U. S. Government Printing Office (1959).
5. M. Farber, M. A. Frisch and H. C. Ko, Trans. Faraday Soc. 65, 3202 (1969).

APPENDIX I

THERMAL DECOMPOSITION OF 1,3,5,7-TETRANITRO-1,3,5,7-TETRAAZACYCLOOCTANE (HMX)

Milton Farber and R.D. Srivastava
Space Sciences, Inc.
Monrovia, California

The sublimation and thermal decomposition of HMX were studied experimentally by means of Langmuir evaporation and effusion mass spectrometry in the temperature range 175 to 275 C. The Langmuir evaporation mass spectrometry results indicated simultaneous sublimation and thermal decomposition of HMX. In addition to HMX, the major decomposition product observed was the $C_2H_4N_4O_4$ (148 amu) molecule. Gas phase decomposition within the effusion cell produced numerous smaller molecules and free radicals. In all cases these were derivable from the further decomposition of the 148 amu molecule. No peaks at 249 or 250 were observed, indicating that HMX does not initially decompose by splitting off an NO_2 group nor that elements attached to the ring migrate to adjacent groups to split off HNO_2. An activation energy of 175 kJ/mol (42 kcal/mol) was obtained for the thermal decomposition of HMX in the effusion cell experiments. The Langmuir experiments showed that the primary mechanism for the thermal decomposition is ring cleavage to two equal 148 amu species.

INTRODUCTION

Several mechanisms for the thermal decomposition of 1,3,5,7-tetranitro-1,3,5,7-tetraazacyclooctane (HMX) have been proposed. These include ring cleavage of the C—N bonds, splitting off NO_2 groups and atomic migration from ring attached groups.[1,2] To obtain a clearer definition of the mechanisms, the sublimation and thermal decomposition of HMX in the temperature range 175 to 275 C were investigated mass spectrometrically at this laboratory. Two techniques, the Langmuir evaporation and the effusion, were employed in these studies. This allowed the initial gas phase products to be observed within a few microseconds, as well as observation of further decomposition products produced within effusion cell reactions. Several experimental precautions were taken to ensure that the gaseous products observed were from parent precursors and not from electron impact within the ionization chamber of the mass spectrometer. The identification of the products in short times allowed a proposed mecha. ism for HMX thermal decomposition.

EXPERIMENTAL APPARATUS AND PROCEDURES

The sublimation and thermal decomposition studies of HMX were conducted by both the effusion-mass spectrometric and the Langmuir evaporation-mass spectrometric methods. In the effusion experiments the material is placed within an effusion cell having a small orifice (less than 1 mm diameter) which allows the pressure of the gas produced from evaporation or decomposition to be much higher (three or more orders of magnitude) within the cell than the surrounding vacuum (see Fig. 1). The gas products collide with each other, the cell walls and with the condensed phase many times prior to their effusing from the cell into the mass spectrometer chamber. This may cause secondary decomposition and fragmentation.

The evaporation (Langmuir) method is one in which the material is heated within the main vacuum chamber and allowed to enter the mass spectrometer chamber without further decomposition or collision with other gaseous molecules.

Details of the dual vacuum chamber-quadrupole mass spectrometer system (Fig. 1) used in these experiments have been presented previously.[3] The samples were contained in an alumina effusion cell 25 mm long, with an inside diameter of 6.8 mm; an elongated orifice 0.75 mm in diameter by 5.5 mm long was employed for beam collimation. The cell was positioned within 5 cm of the ionization chamber of the mass spectrometer, allowing species leaving the solid or liquid surface to be measured within 10 microseconds. The alumina cell was heated by a resistance furnace and temperature measurements were made by means of thermocouples imbedded in the cell body. The ion intensities were identified by their masses, isotopic distributions, and appearance potentials. The method of determining the mass spectrometer resolution, as well as the measurement of the isotopic abundance ratios, has been presented previously.[4] The resolution of the mass spectrometer is 1 in 500. ^{127}I and $^{254}I_2$ were employed for amu calibration. All quadrupole experimental mass discrimination effects were taken into account and the necessary corrections to ion intensity pressure relationships were made. Only the chopped, or shutterable, portions of the intensities were recorded, since the mass spectrometer was equipped with a beam modulator and a phase sensitive amplifier. Ion currents, which originated from species in the molecular beam, appeared as a 30 c/s square wave while background gases continued to exist as a d.c. current. An a.c. current could be observed in a d.c. signal 1000 times greater.

It was necessary to ascertain with a high degree of confidence that the measured ion intensities were those from the parent species and not from the fragments of the larger molecules. Therefore, the mass spectrometer was operated at an ionizing voltage 1 to 2 eV above the appearance potential, which in nearly all cases allows only the formation of the ion from the parent species since a fragmentation process occurs at higher ionization voltages.[5-8] The ionization energies employed were between 14 and 18 eV.

The formation of an ion from its parent precursor requires a lower

ionization energy than for an ion formed from fragmentation of a larger molecule. For example, to produce NO_2^+ from $(CH_3)_2NNO_2$ (14.6 eV) requires approximately 5 eV more than from $NO_2 \longrightarrow NO_2^+$ (9.75 eV).[9]

High electron impact energies can produce species within the mass spectrometer that are not related to the combustion processes. Figure 2 illustrates this effect on HMX decomposition products. At an energy of 50 eV a number of peaks are seen, which disappear at 30 eV. The fragmentation of the nitramine ring requires a higher electron impact energy than that required for the removal of a group attached to the ring by a single bond. The formation of ions within the ionization chamber of the mass spectrometer is shown in Fig. 3. NO_2^+ and N_2O^+ are produced at electron energies above 20 eV. Thermal effects on the ionization processes are negligible in the temperature range of these studies.

RESULTS

As reported in the previous section, the sublimation and thermal decomposition of HMX were studied in the temperature range 175 to 275 C by means of the Langmuir evaporation and effusion methods, and species produced were identified mass spectrometrically.

These experiments showed sublimation taking place at temperatures as low as 175 C. Results from fairly low temperature effusion cell measurements by Rosen and Dickinson[10] and by Crookes and Taylor[11] indicate that HMX evaporates without appreciable decomposition. Rosen and Dickinson reported a vapor pressure range of 10^{-11} to 10^{-10} atm in the temperature range 98 to 130 C, and Crookes and Taylor determined vapor pressure data varying from 10^{-7} to 10^{-5} atm in the temperature range 188 to 213 C. Our cell evaporation and decomposition pressures varied from 5×10^{-7} to 5×10^{-3} atm in the temperature range 175 to 275 C.

The Langmuir evaporation experiments of HMX indicated sublimation and thermal decomposition occurring simultaneously. An example of these results is presented in Fig. 4, which shows relative concentrations of the HMX molecule at 296 amu and its decomposition product at 148 amu. No other fragments were observed from the decomposition of HMX, which was directly heated in vacuum.

The effusion experiments allowed further decomposition of the gas phase molecules as a result of numerous reactions with the walls

and with the condensed phase. Between 175 and 200 C the sublimation of HMX was predominant. Figure 5 shows the relative intensity of HMX at 200 C, with a smaller relative concentration appearing at 222 amu. As the temperature approached 225 C considerable decomposition occurred (Figs. 6 and 7). Relative concentrations at 148, 128, 120, 102, 74 and 56 amu are depicted in Fig. 6. The peaks appearing in the low 18 to 46 amu range are shown in Fig. 7.

DISCUSSION

The direct evaporation in vacuum (Langmuir experiments) allowed any species derived from the condensed phase to enter the mass spectrometer without prior collision with any other species or with the surface area. From these experiments the mechanism proposed for the primary mode of solid phase HMX decomposition is ring cleavage, as

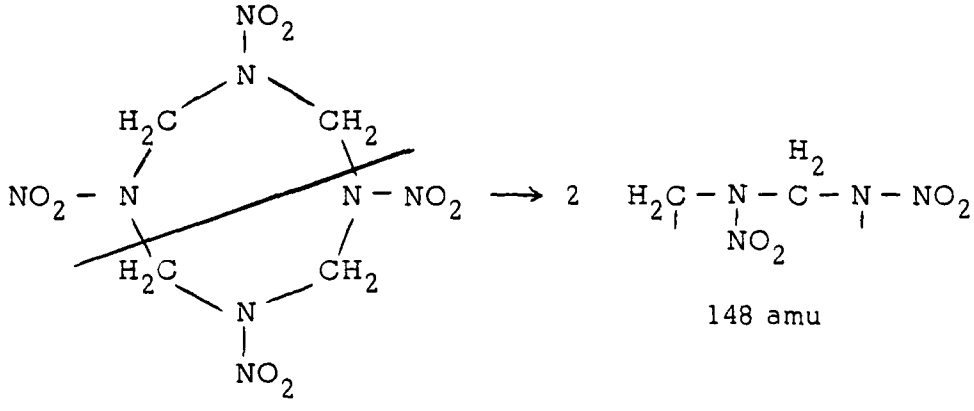

296 amu

148 amu

The 148 amu fragment may form a more stable molecule by the joining of the split C and N bonds, resulting in

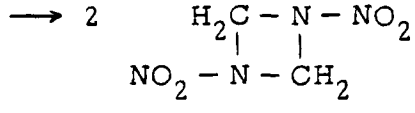

148 amu

The products of sublimation and decomposition within the effusion cell undergo further decomposition to form the products shown in Figs. 6 and 7.

The effusion cell decomposition products shown in Fig. 5 include a small relative quantity of a molecule or radical at 222 amu. This would indicate a decomposition mode as

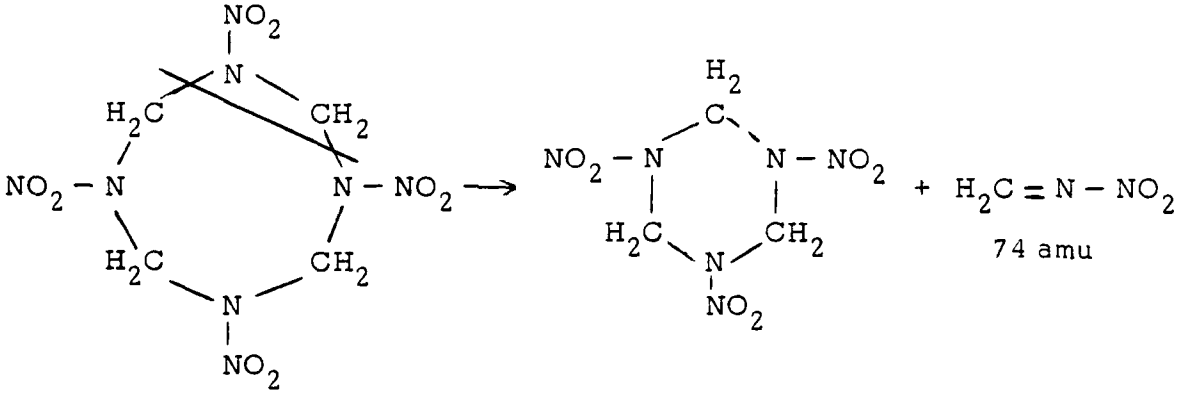

296 amu 222 amu 74 amu

The peaks shown in Figs. 6 and 7 may result from further decomposition of the major product at 148 amu through collisions within the cell. The reaction scheme is either

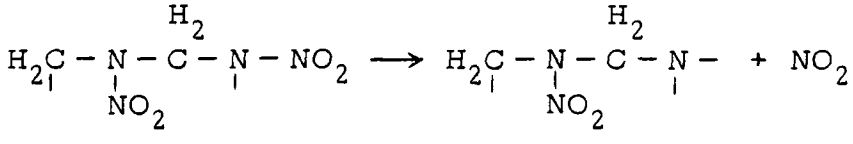

148 amu 102 amu

or, from the bond closure molecule,

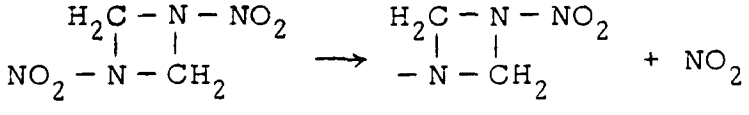

102 amu

The 102 fragment splits off another NO_2 group, yielding

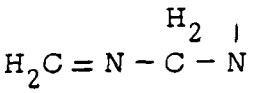

56 amu

which can rearrange to form a more stable resonating molecule,

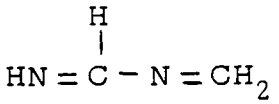

56 amu

This molecule can split to produce two $H_2C=N\cdot$ radicals. The 148 amu fragment can also split into two equal stable molecules,

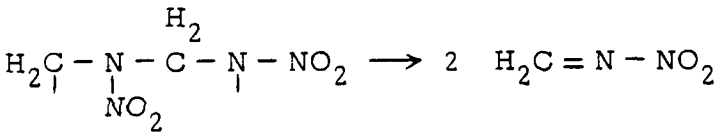

148 amu 74 amu

The peaks at 120 amu, $CH_2N_3O_4$, and at 128 amu, $C_3H_2N_4O_2$, are apparently produced in the effusion cell as a result of the reaction of the gaseous products with the condensed phase and with each other. These peaks have also been observed by Goshgarian,[1] Stals,[12] and Suryanarayana, et al.[13]

Goshgarian[1] has postulated the formation of the 128 amu peak as

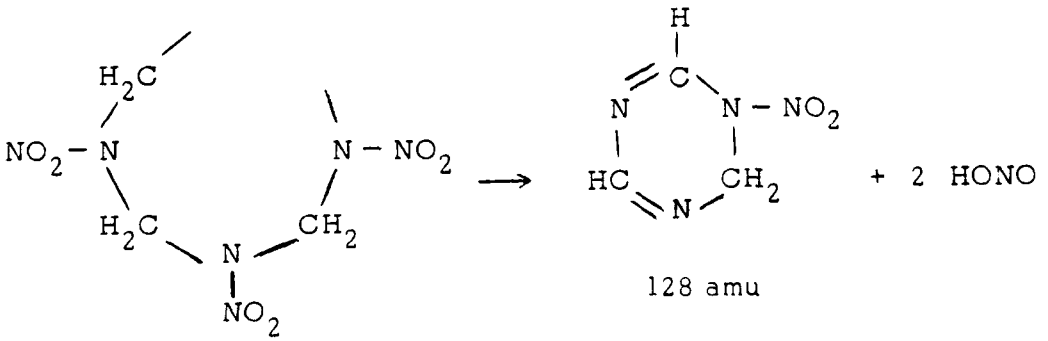

222 amu 128 amu

The peak at 120 amu has been postulated by Stals[12] as ring migration of the NO_2 group,

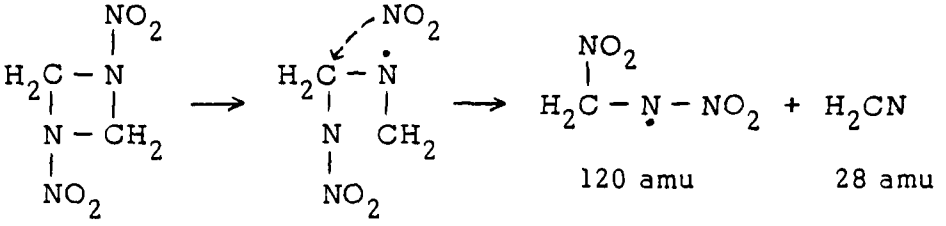

148 amu

120 amu + 28 amu

Stals also indicated that the formation of the 132 peak results from the 148 molecule losing an O atom,

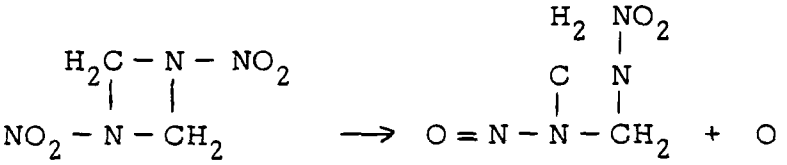

148 amu → 132 amu

Beyer[14] in ESR studies found considerable free radicals produced from the decomposition of HMX at 260 C. He attributed this free radical spin resonance to the formation of $H_2CN\bullet$ at 28 amu. Figure 7 shows a high concentration of the 28 amu peak which, in all probability, is a mixture of the decomposition products CO, N_2, and H_2CN. He postulated that the radical, H_2CN, is derived from

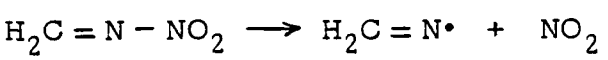

74 amu → 28 amu

The possibility of ring migration to form HNO_2 has been raised by Shaw and Walker.[2]

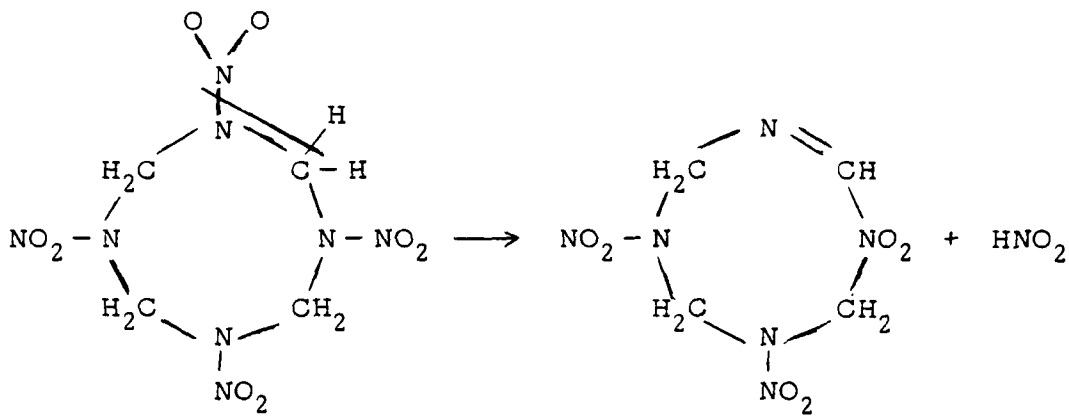

296 amu 249 amu

The ring migration can result in either of two bond configurations:

$$HNO_2 \longrightarrow O-N-O-H \quad \text{or} \quad O-\underset{\underset{H}{|}}{N}-O$$

However, no evidence of such migration has been found in the experiments at this laboratory, since the 249 amu peaks were not observed. Also, N – N bond rupture to produce NO_2 species does not appear to be a likely primary decomposition mode, since the peak at 250 amu was not observed in these studies and those by others.[1]

Our studies yielded an activation energy of 175 kJ/mol (42 kcal/mol) for the decomposition to NO_2 groups, as shown in Fig. 8. Goshgarian[1] reported activation energies of 159 ± 8 kJ/mol (38 ± 2 kcal/mol) from 250 to 270 C and 175 ± 8 kJ/mol (42 ± 2 kcal/mol) from 271 to 280 C. McGuire[15] reported an Ea of 175 kJ/mol (42 kcal/mol) from the decomposition of HMX to

$$H_2C=N-NO_2$$

74 amu

The enthalpy of sublimation obtained by Taylor and Crookes[11] was 163 kJ/mol (39 kcal/mol), also shown in Fig. 8.

The proposed primary thermal decomposition mechanism of the cleavage of the HMX molecule into equal fragments of 148 amu is compatible with thermodynamic considerations. The very high specific heat of the solid HMX compound allows adsorption of sufficient enthalpy to cause the rupturing of the C– N bonds of the highly strained ring configuration. It has been calculated[2] that the C–N bond strength due to ring strains is 25 kcal/mol less than the normal C–N bond strength in aliphatic amines.

ACKNOWLEDGMENT

This research was supported by the Department of the Navy, Office of Naval Research, Material Sciences Division, Power Program. Approved for public release; distribution unlimited. Reproduction in whole or in part is permitted for any purpose by the United States Government.

REFERENCES

1. B. B. Goshgarian, Final Report AFRPL-TR-78-76, October 1978, Air Force Rocket Propulsion Laboratory, Edwards AFB, Ca.
2. R. Shaw and F. E. Walker, J. Phys. Chem. 81, 2572 (1977).
3. M. Farber, M. A. Frisch, and H. C. Ko, Trans. Faraday Soc. 65, 3202 (1969).
4. M. Farber and R. D. Srivastava, Combustion and Flame 20, 33 (1973).
5. M. Farber, R. D. Srivastava, and O. M. Uy, J. Chem. Soc. Faraday Trans. I 68, 249 (1972).
6. M. Farber and R. D. Srivastava, J. Chem. Soc. Faraday Trans. I 70, 1581 (1974).
7. M. Farber and R. D. Srivastava, J. Chem. Soc. Faraday Trans. I 73, 1692 (1977).
8. M. Farber and R. D. Srivastava, Chem. Phys. Lett. 51, 307 (1977).
9. H. M. Rosenstock, K. Draxl, B. W. Steiner and J. T. Herron, "Energetics of Gaseous Ions," J. Phys. Chem. Ref. Data, Vol. 6, 1977 (Supplement No. 1).
10. J. Rosen and C. Dickinson, J. Chem. Eng. Data 14, 120 (1969).

11. J.W. Taylor and R. J. Crookes, J. Chem. Soc. Faraday Trans. 1, 72, 723 (1976).
12. J. Stals, Trans. Faraday Soc. 67, 1768 (1971).
13. B. Suryanarayana, T. Axenrod, and G.W.A. Milne, Org. Mass Spec. 3 (1970).
14. R. A. Beyer, Conference on Thermal Decomposition, USAF Academy, Colorado, August 1979.
15. R. McGuire, Conference on Thermal Decomposition, USAF Academy, Colorado, August 1979.

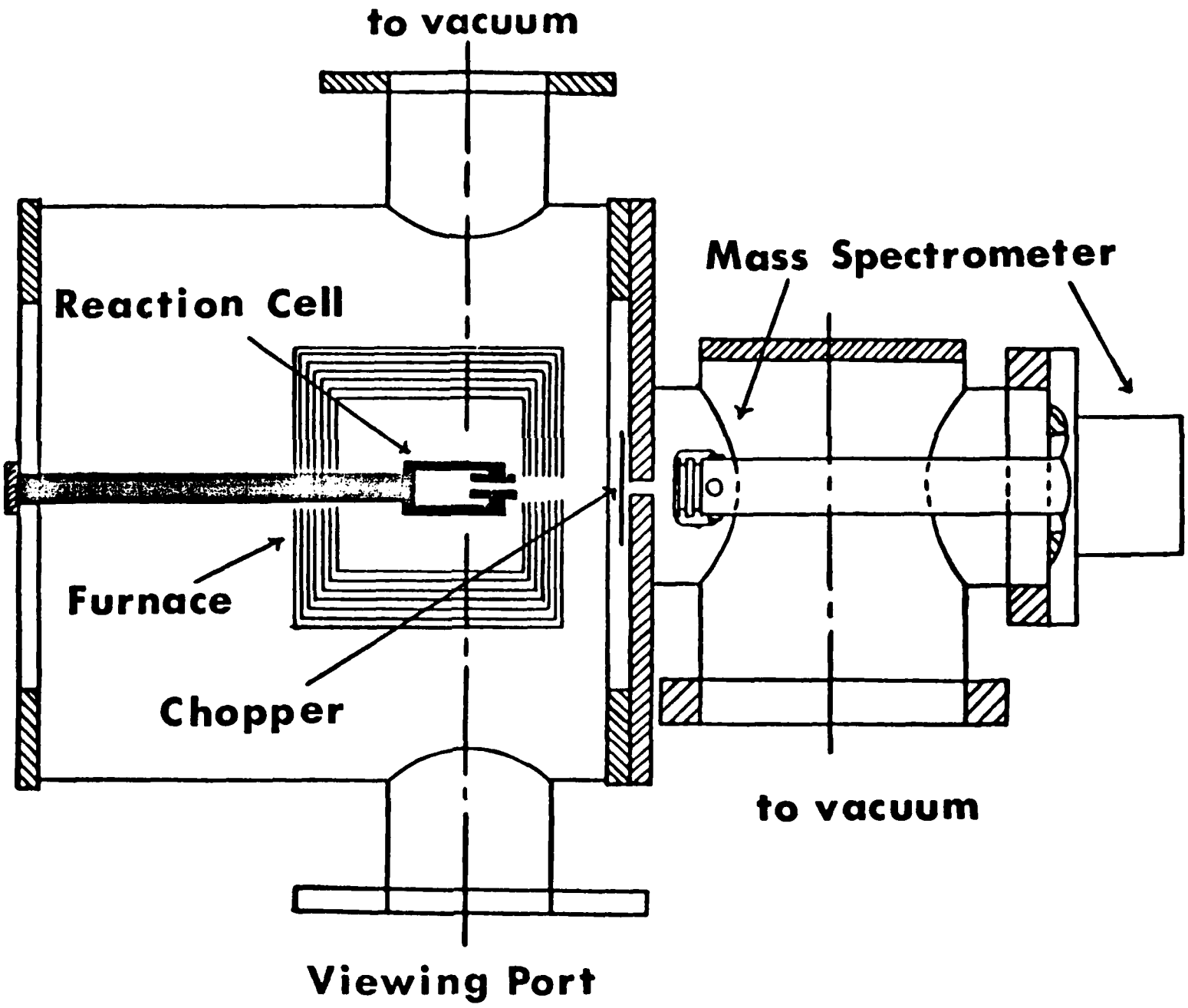

Fig. 1. Dual Vacuum Mass Spectrometer System

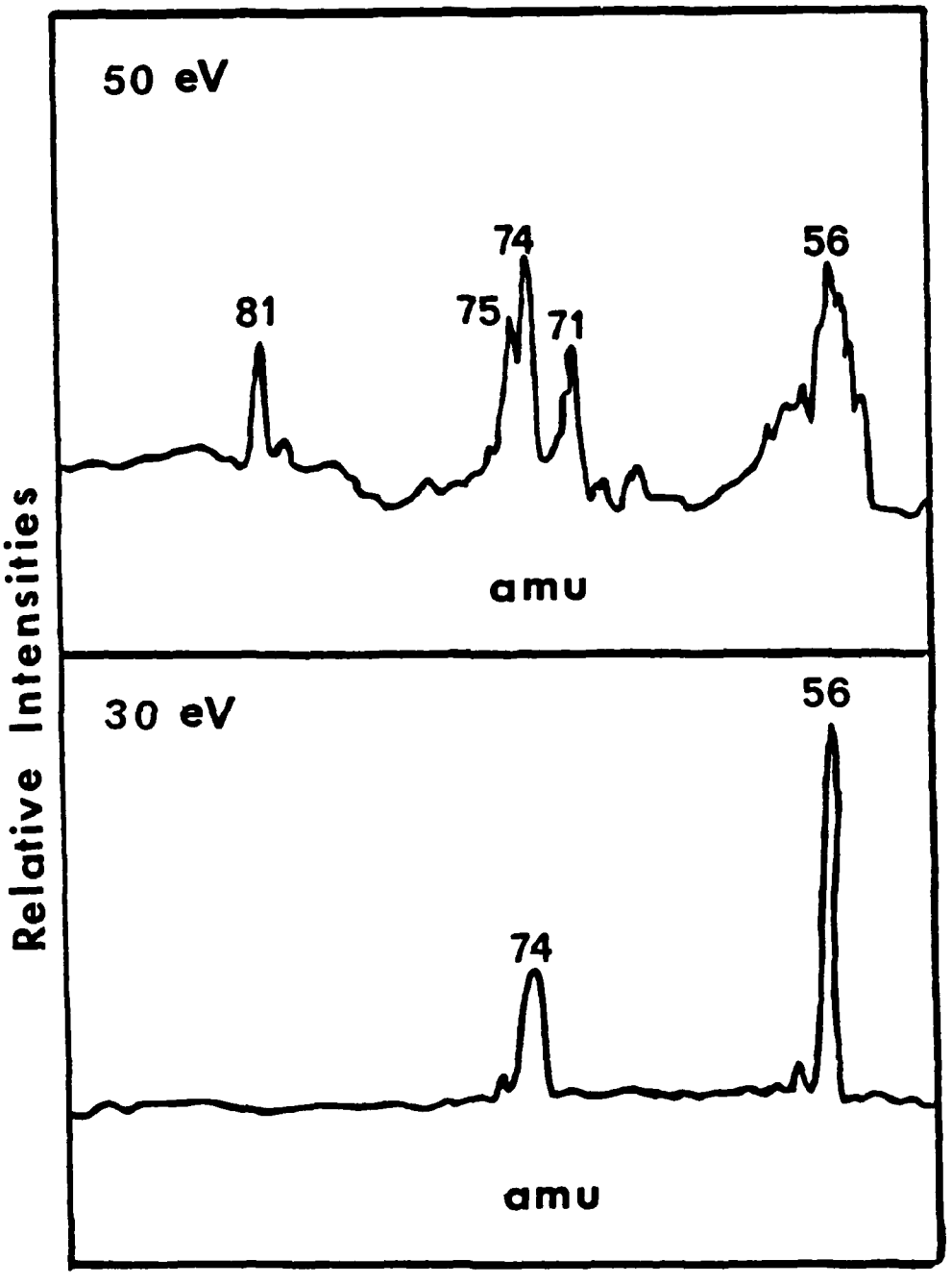

Fig. 2. Thermal Decomposition of HMX in an Effusion Cell at 225 C as a Function of Electron Impact Ionizing Energy

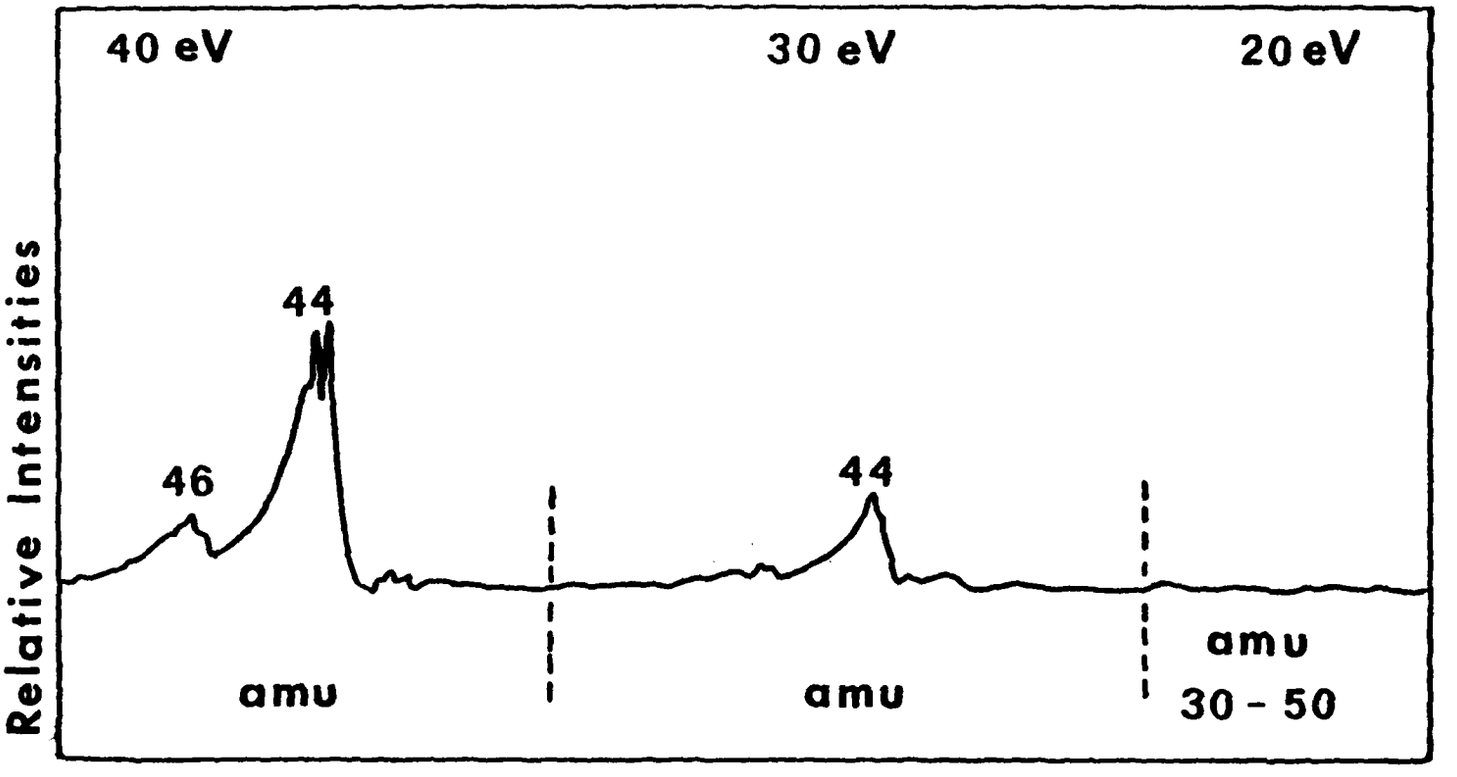

Fig. 3. Langmuir Evaporation of HMX at 220 C

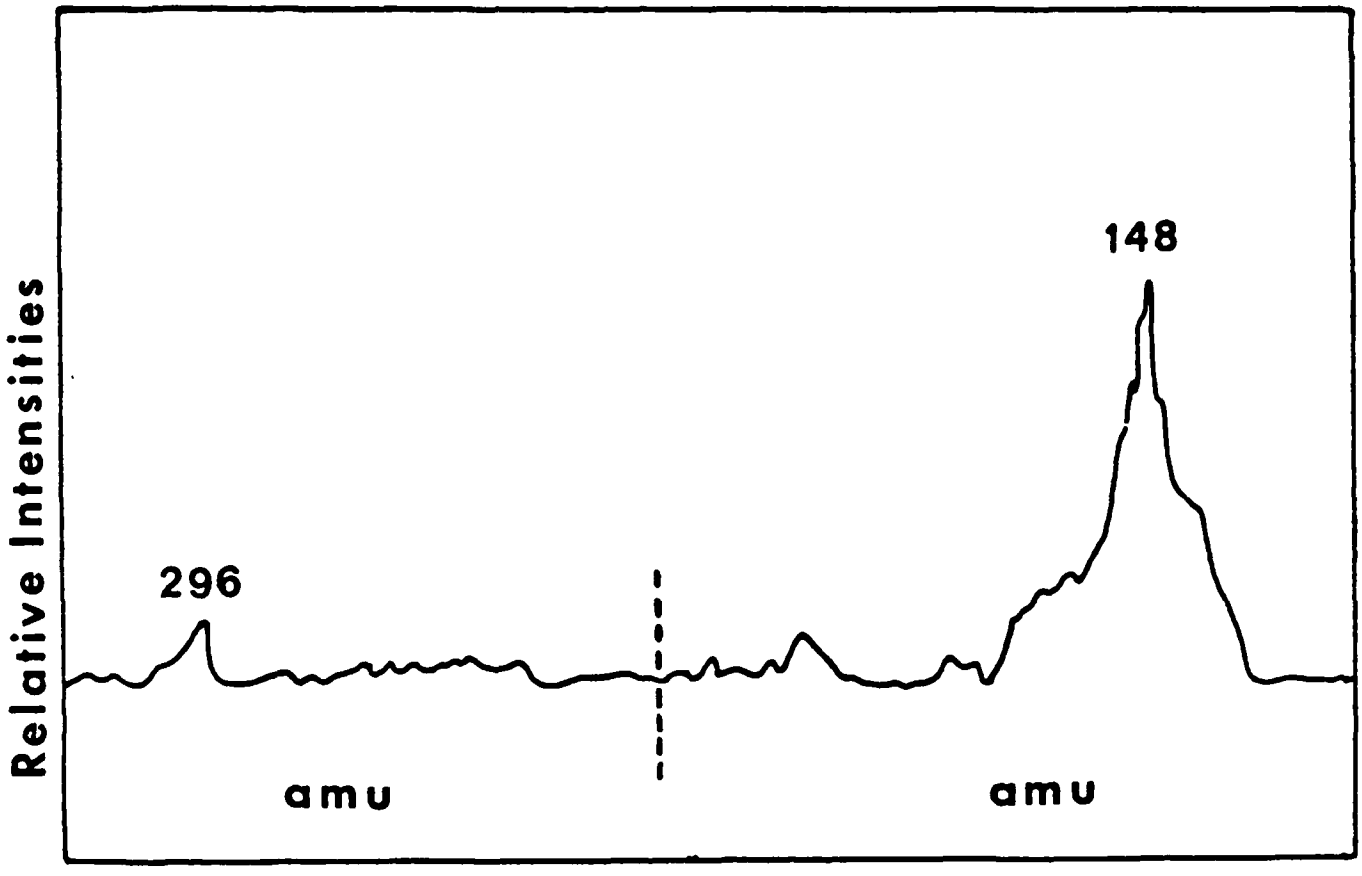

Fig. 4. Langmuir Evaporation of HMX at 200 C

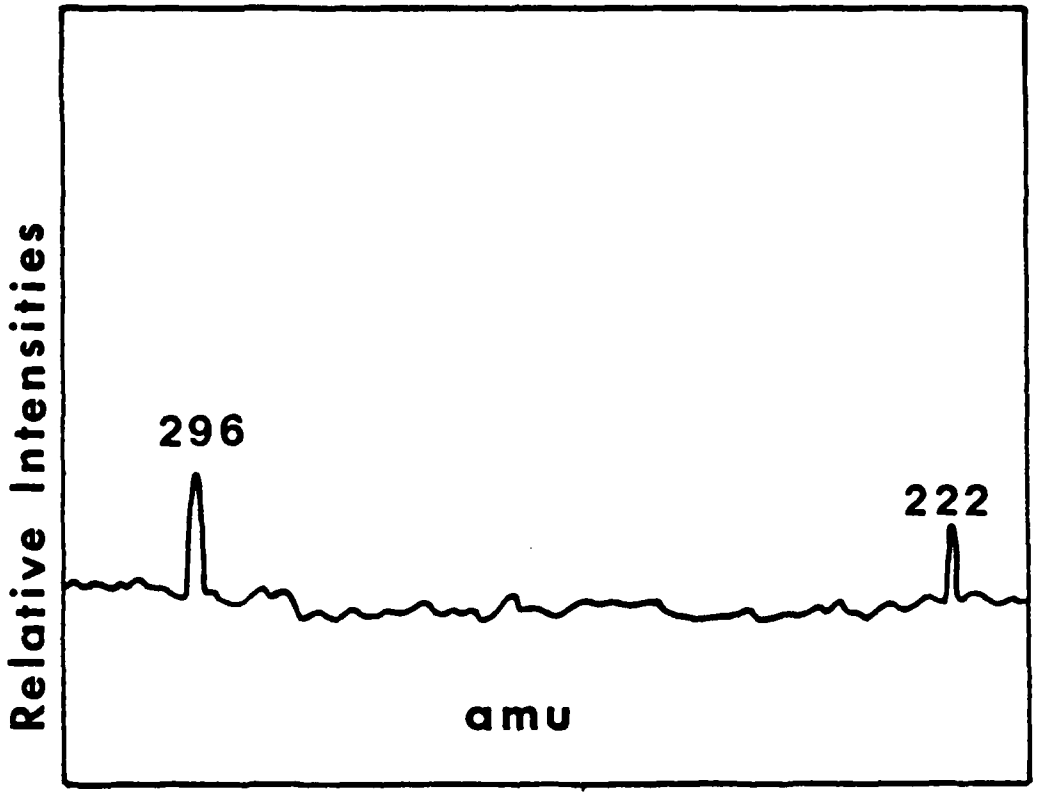

Fig. 5. Evaporation and Thermal Decomposition of HMX in an Effusion Cell at 200 C

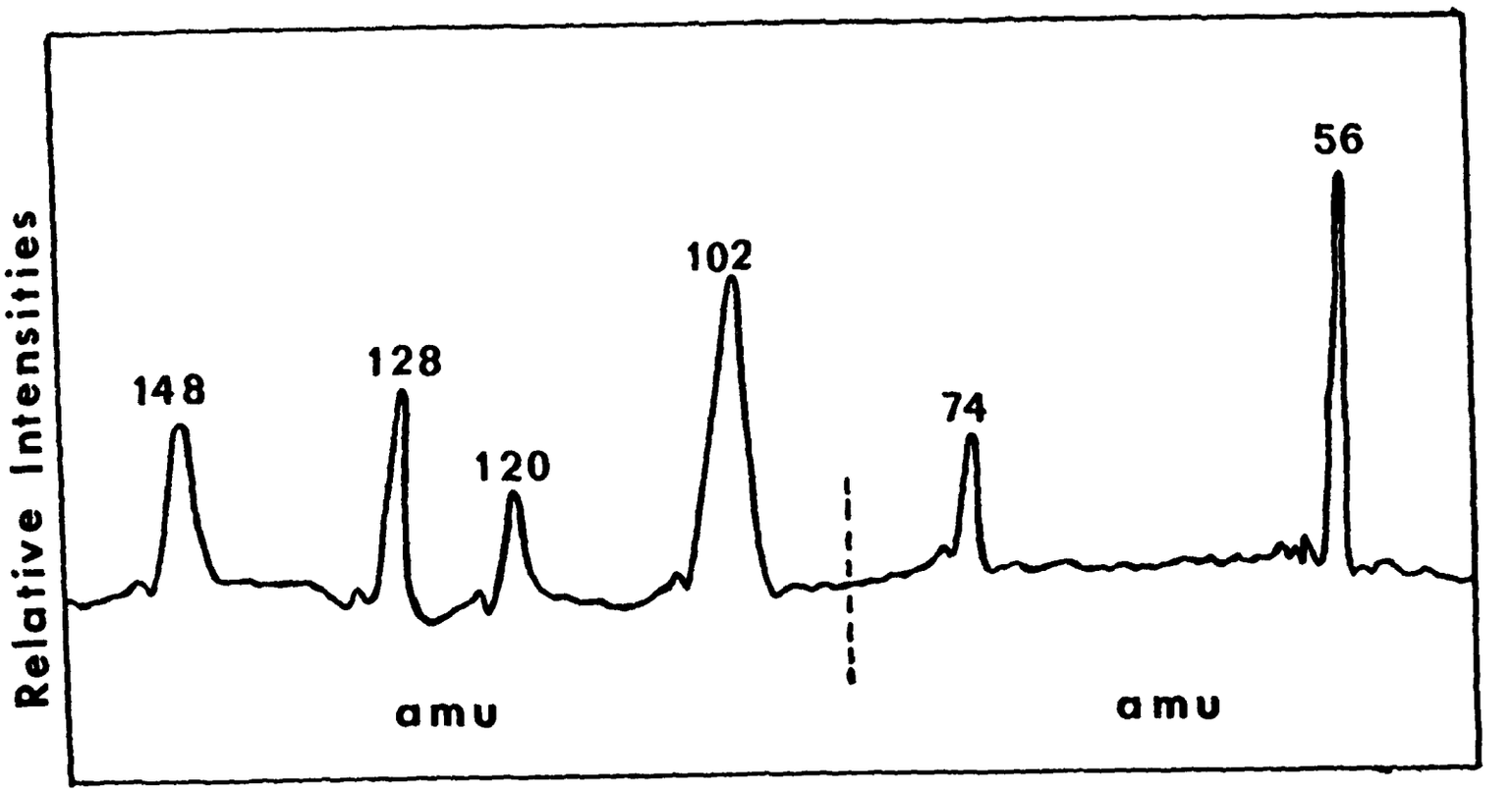

Fig. 6. Thermal Decomposition of HMX in an Effusion Cell at 225 C

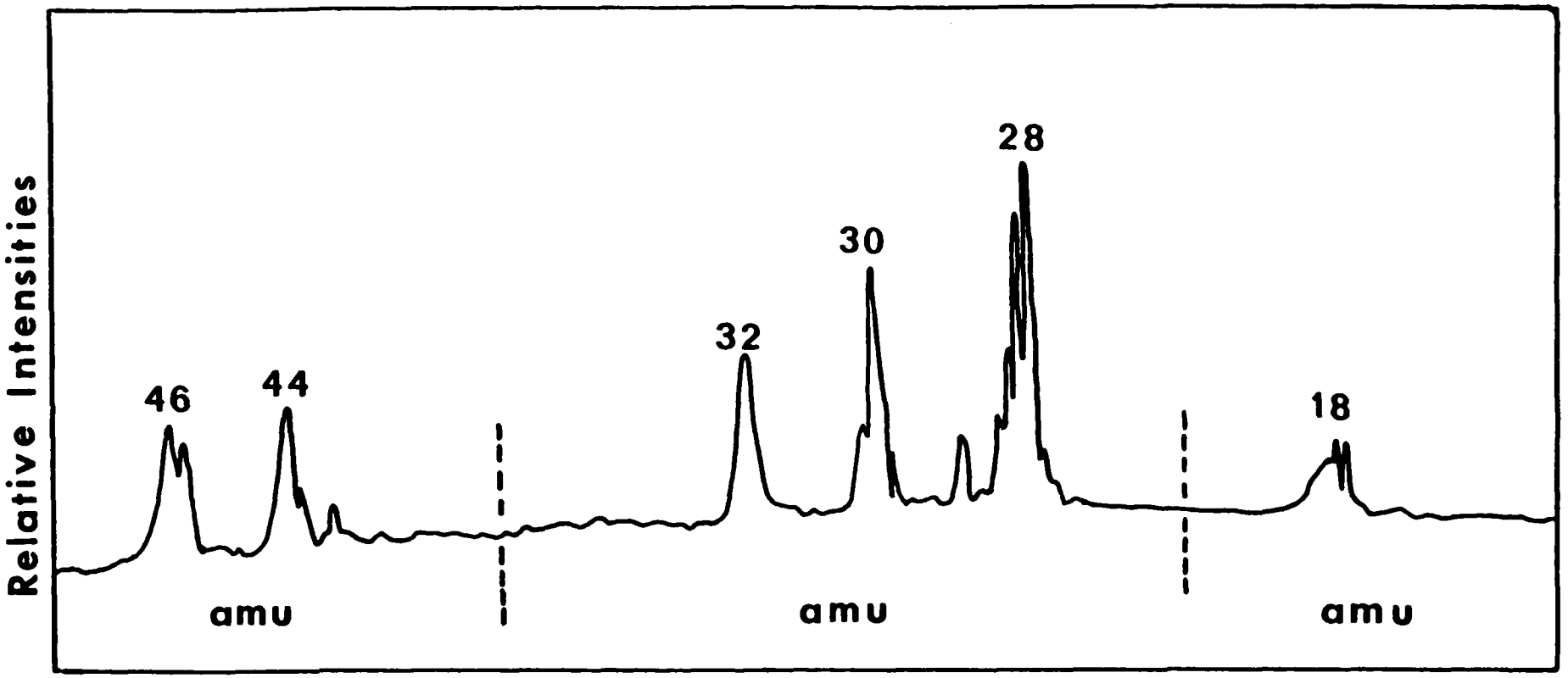

Fig. 7. Thermal Decomposition of HMX in an Effusion Cell at 225 C

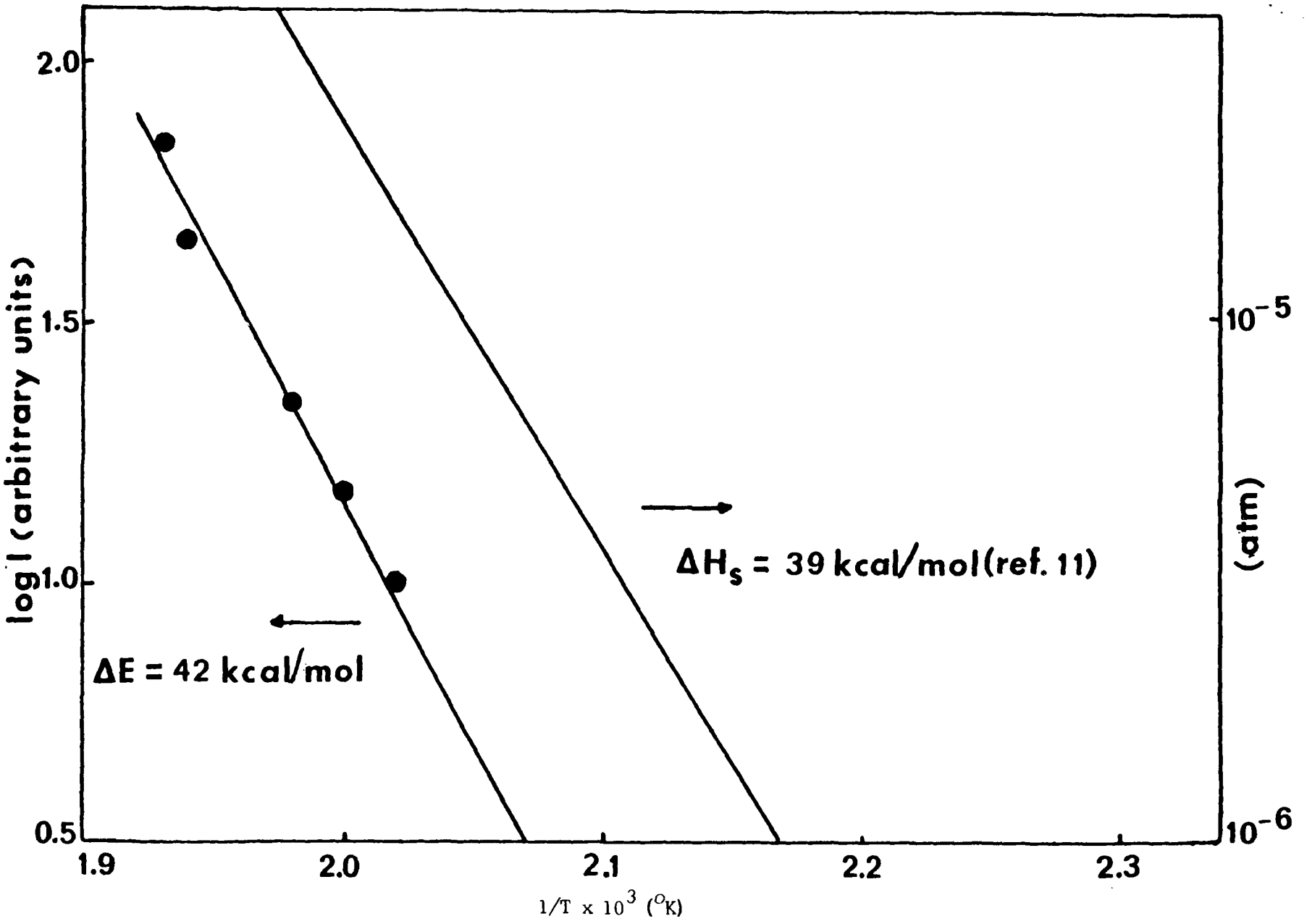

Fig. 8. Temperature Dependence of NO_2 from the Thermal Decomposition of HMX in an Effusion Cell

APPENDIX II

THERMAL DECOMPOSITION OF 1,3,5-TRIAMINO-2,4,6-TRINITROBENZENE*

Milton Farber and R. D. Srivastava
Space Sciences, Inc., Monrovia, California

The products of sublimation and thermal decomposition of 1,3,5-triamino-2,4,6-trinitrobenzene have been determined mass spectrometrically in the temperature range 200 - 300 C employing both the effusion and Langmuir evaporation methods. Electron impact ionization energies 1 - 2 eV above appearance potentials were employed to eliminate fragmentation of larger species. The unusual crystal structure of TATB results in long C—C bonds, with considerable hydrogen bonding. At 250 C the molecule sublimed readily, with some thermal decomposition, causing the splitting of the molecule into two fragments at amu 144 and 114. Further fragmentation of these species to lower amu molecules occured. The effusion experiments produced numerous low molecular weight species, indicating that the initial radicals were relatively shortlived.

*This research was supported by the Department of the Navy, Office of Naval Research, Material Sciences Division, Power Program.

INTRODUCTION

1,3,5,-triamino-2,4,6-trinitrobenzene (TATB) has been described as an unusual molecule (1,2). The unusual crystallographic structure of the molecule, with its extremely large C–C bond lengths and inter- and intramolecular hydrogen bonding, results in considerable thermal decomposition as well as its molecular evaporation. Its structure is quite distorted, with C–C distances of 1.441 Å units, considerably larger than the average C–C bond lengths in other benzene rings (1). It has no observable melting point (2). Its activation energy has been reported by Bailey (3) as 250.6 kJ/mole, its heat of formation as -154.2 kJ/mole by Hardesty and Kennedy (4), and its heat of sublimation as 168.3 kJ/mole by Shaw (5) and by Rosen and Dickinson (6). Vacuum sublimation studies by the Langmuir technique were conducted by Rosen and Dickinson (6) in the temperature range 129.3 to 177.3 C, with vapor pressures of $7.33 \times 10^{10-8}$ and 1.67×10^{-5} mm Hg, respectively.

Identification of the products formed from the thermal decomposition of TATB has not heretofore been reported, although the rates of decomposition and activation energies based on overall heat and weight loss of the solid phase material have been determined in several studies (1,2,7,8). Therefore, the investigation at this laboratory was undertaken to definitively identify these products and thereby derive a mechanism for the initial solid phase decomposition. Two mass spectrometric techniques were employed: the evaporation (Langmuir experiment) method, and the effusion (modified Knudsen cell) method.

EXPERIMENTAL APPARATUS AND PROCEDURES

In effusion experiments the material is placed within an effusion cell having a small orifice (less than 1 mm diameter) which allows the pressure of the gas produced from evaporation or decomposition to be much higher (3 or more orders of magnitude) within the cell than the surrounding vacuum (see Fig. 1). The gas products collide with each other, the cell walls and with the condensed phase many times prior to their effusing from the cell into the mass spectrometer chamber. This may cause secondary decomposition and fragmentation.

The evaporation (Langmuir) method is one in which the material is heated within the main vacuum chamber and allowed to enter the mass spectrometer chamber without further decomposition or collision with other gaseous molecules.

Details of the dual vacuum chamber-quadrupole mass spectrometer system (Fig. 1) used in these experiments have been presented previously (9). The samples (5 - 25 mg of powdered TATB) were contained in an alumina effusion cell 25 mm long, with an inside diameter of 6.8 mm; an elongated orifice 0.75 mm in diameter by 5.5 mm long was employed for beam collimation. The cell was positioned within 5 cm of the ionization chamber of the mass spectrometer, allowing species leaving the solid or liquid surface to be measured within 10 microseconds after their exit from the cell. The alumina cell was heated by a resistance furnace and temperature measurements were made by means of thermocouples imbedded in the cell body. In the Langmuir experiments the sample was placed in an open alumina shell containing a thermocouple for temperature determination. The method of determining ion intensities, mass spectrometer resolution, as well as the measurement of the isotopic abundance ratios, has been presented previously (10). All quadrupole experimental mass discrimination effects were taken into account and the necessary corrections to ion intensity pressure relationships were made. Only the chopped, or shutterable, portion of the intensities was recorded, since the mass spectrometer was equipped with a beam modulator and a phase sensitive amplifier. The experimental procedure has been described in detail previously (9-14). 127_I and 254_{I_2} were employed for amu calibration. Partial pressures were obtained from the calibrated data by means of the relationship

$$p_i = \frac{I_i (\sigma \gamma)_a}{I_a (\sigma \gamma)_i} p_a$$

where a is the calibrated species and σ and γ are respective ionization cross-sections and electron multiplier corrections.

It was necessary to ascertain with a high degree of confidence that the measured ion intensities were those from the parent species and not from the fragments of the larger molecules. Therefore, the mass spectrometer was operated at an ionizing voltage of 1 to 2 eV above the appearance potential, which in nearly all cases allows only the formation of the ion from the parent species since a fragmentation process usually occurs at higher ionization voltages. The ionization energies employed were between 14 and 18 eV.

Fragmentation of ring constituents requiring the rupture of a single bond by electron impact will occur at lower ionization energies than will fragmentation of the ring itself requiring the rupture of multiple bonds. For example, Fig. 2 shows the effect of electron impact ionization energies on the relative intensities of the parent and single bond fragmentation peaks of the gaseous TATB molecule. At an ionization energy of 50 eV the removal of an NO_2 group from the ring is readily accomplished and produces a fragment at amu 212 approximately half the intensity of the TATB molecule. At 30 eV the fragment peak at amu 212 is only one-third the TATB peak, and at 20 eV is one-sixth the TATB. Finally, at 14 eV, which is only 2 eV above the appearance potential of TATB, the fragment disappears. This appears to be consistent with the fact that an additional electron energy of 5 eV would be required to produce ionization of NO_2 from C–NO_2 fragmentation (15).

RESULTS

The TATB molecule was found to be quite stable, with little vaporization below 200 C; vapor pressure measurements agreed with the results of Rosen and Dickinson (6).

The direct evaporation and decomposition of TATB were studied by the Langmuir method, in which the TATB was directly heated in a high vacuum (10^{-8} atm) in the temperature range 200 - 300 C. At 250 C the molecule sublimed readily, with some thermal decomposition. The decomposition intensities increased with increasing temperature, as did the sublimation. A typical mass spectrum of the products of sublimation

and decomposition is presented in Fig. 3. The molecule at amu 258 is the dominant species, with decomposition products appearing at lower concentrations.

The Knudsen method was employed to study the decomposition products at much higher intensities resulting from beam collimation and from a higher effusion cell pressure (approximately 0.1 mm Hg, several orders of magnitude greater than the Langmuir method). The relative intensities of the decomposition products varied from experiment to experiment and with time, with no attempt made to obtain quantitative data. At 250 C considerable decomposition of the TATB molecule was produced within the effusion cell. The entire mass range from 1 to 258 amu was scanned. The decomposition product with the largest mass number was the amu 144 species. Examples of other large fragments from the effusion cell experiments appearing at mass numbers 128, 114, and 98 at 250 C, are shown in Fig. 4. The molecule appears to initially fragment into two unequal mass fragments. Due to the higher pressures within the effusion cell, species monitored by the mass spectrometer had a higher intensity than those from the Langmuir evaporation. A comparison of the species intensities at 250 C is presented in Table 1. The primary purpose of the study was to identify the species as they first appeared in a measurable quantity, 10^{-10} atm partial pressures or greater, and thereby deduce the mechanism for the solid state decomposition. The decomposition products from the effusion cell experiments varied considerably with temperature, indicating gas phase and gas-solid phase decomposition within the cell. The variation in intensity with increasing temperature of one of the larger fragments of decomposition, the amu 114 species, indicates an activation energy of 179.9 kJ/mole.

The products within the effusion cell continued to decompose into smaller species, which were observed in fairly large concentrations. Relative concentrations of these species in the low amu range at 250 C, which include H_2, NH_2, H_2O, CO, NO, CO_2 and NO_2, are presented in Table 1.

DISCUSSION

Since the Langmuir experiments allowed a free sublimation, and

probably minimized collisions of the decomposition radicals, those data were employed to determine the decomposition mechanism. Qualitatively, nearly equal amu 144 and 114 peaks were observed (Fig. 3 and Table 1). Thus the primary decomposition mechanism is ring cleavage,

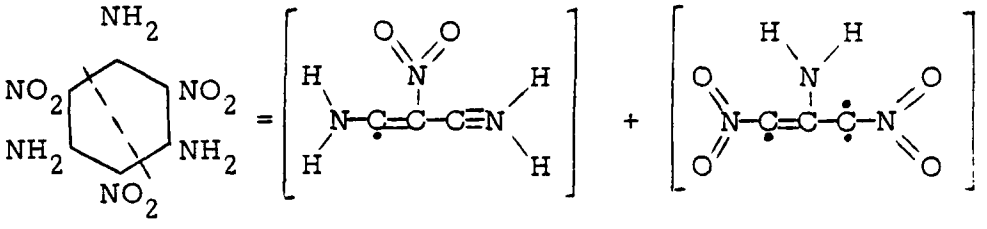

amu 114 amu 144

The amu 144 species is in all probability a reactive radical with a short lifetime. The amu 114 molecule is probably more stable, which may account for its much larger concentration in the effusion experiments. Although mass spectrometer sampling is fast (within 10 to 50 microseconds), further decomposition may occur within the mass spectrometer ionization chamber. This would explain the amu 128 peak observed in the Langmuir experiments produced from the larger amu 144 radical.

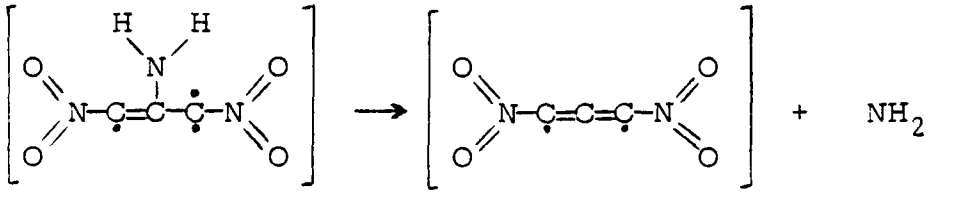

amu 144 amu 128 amu 16

The amu 128 species, $C_3N_2O_4$, may be more stable through double bond resonance than the amu 144 radical, accounting for its larger concentration.

In the same manner the amu 114 product can further decompose, also losing an amine group, to produce the prominent peak at amu 98,

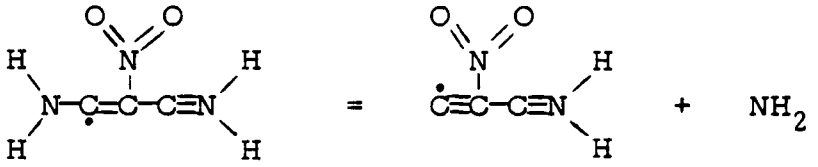

amu 114 amu 98 amu 16

A peak at amu 86 was observed; its relative intensity is given in Table 1. This species could be produced in one of three possible decomposition processes. Ring cleavage into two fragments, at 86 amu and at 172, is rather unlikely since the amu 172 species was not observed in either study.

There is the possibility that the prominent amu 86 species may occur from ring splitting. This would require the release of three equal species simultaneously

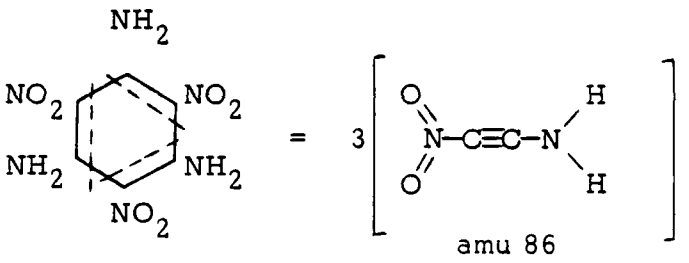

amu 86

The formation of the amu 86 species is more likely a result of the decomposition of the amu 144 radical

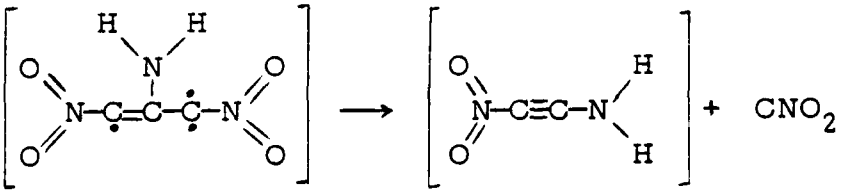

amu 144 amu 86 amu 58

Since further decomposition occurs in the gas phase within the effusion cell, the peak at amu 70 may result from the amu 86 species losing a NH_2 group.

From the studies at this laboratory it appears certain that decomposition of solid TATB produces radicals. The radicals may or may not have long half-lives since they are sampled by the mass spectrometer in less than a millisecond after exiting the cell. Continued collisions within the effusion cell probably produce smaller stable fragments. Britt and Moniz (7) have studied, by means of electron spin resonance, the formation of free radicals resulting from irradiation by ultraviolet of TATB. They recently reported that a considerable concentration of unknown free radicals was observed by means of ESR of the thermal decomposition of TATB at a temperature of 350 C and at a pressure of 1 atm (7). The free radicals identified mass spectrometrically at this laboratory were obtained at somewhat lower temperatures and at pressures less than 10^{-4} atm.

Sublimation and thermal decomposition results have been reported by Cady and Larson (2), who investigated the structure of the solid TATB molecule. From crystallographic experiments they determined the structure and bond lengths (in Å units) as shown in Fig. 5. As can be seen, the bond lengths are distorted, with a considerable amount of hydrogen bonding both within the molecule and to adjacent molecules. Considerable hydrogen bonding and ring stretching was also reported by Deopura and Gupta (1). Pertaining to the unusual behavior of the molecule, Cady and Larson (2) commented that it contained extremely long C–C bonds in the benzene ring, very short C–N bonds, and six bifurcated hydrogen bonds. The average bond lengths are: C–C 1.441; C–N (nitro) 1.422; C–N (amino) 1.316; and N–O 1.243 (Å). Thermal decomposition would be expected as a result of the stretched bonds in the unusual structure, as determined in the mass spectrometer studies at this laboratory and thermal decomposition experiments employing ESR and DSC. The fairly high enthalpy introduced into the solid as a result of the high specific heat (estimated at between 100 and 125 cal/deg/mole) apparently is sufficient to provide the necessary energy for the rupturing of these highly distorted bonds.

In summary, the proposed mechanism for the decomposition of TATB was derived from the mass spectrometer data. The solid phase molecule absorbed a considerable amount of enthalpy and then ruptured, releasing the products observed. The proposed mechanism is consistent with the imprecise, and very high, melting point of TATB (approximately 450 C), crystallographic spectra, and free radicals reported from ESR experiments.

ACKNOWLEDGMENT

The authors are grateful to Dr. Richard S. Miller of the Office of Naval Research for his very helpful comments during the course of these studies.

REFERENCES

1. Deopura, B. L., and Gupta, V. D., J. Chem. Phys. 54, 4013 (1971).
2. Cady, H. H., and Larson, A. C., Acta Crystallog. 18, 485 (1965).
3. Bailey, P. B., Combust. Flame 23, 329 (1974).
4. Hardesty, D. R., and Kennedy, J. E., Combust. Flame 28, 45 (1977).
5. Shaw, R., J. Phys. Chem. 75, 4047 (1971).
6. Rosen, J., and Dickinson, C., J. Chem. Eng. Data 14, 120 (1969).
7. Britt, A. D., and Moniz, W. B., Conference on Thermal Decomposition, USAF Academy, Colorado, August 1979.
8. J. L. Janney and R. N. Rogers, 1980 Annual Conference on Testing Methods for Propullants and Explosives, Fraunhofer Institut fur Treib- und Explosivstoffe, D7507 Pfinztal-Berghausen, Germany.
9. Farber, M., Frisch, M. A., and Ko, H. C., Trans. Faraday Soc. 65, 3202 (1969).
10. Farber, M., and Srivastava, R. D., Combust. Flame 20, 33 (1973).
11. Farber, M., Srivastava, R. D., and Uy, O. M., J. Chem. Soc. Faraday Trans. I 68, 249 (1972).
12. Farber, M., and Srivastava, R. D., J. Chem. Soc. Faraday Trans. I 70, 1581 (1974).
13. Farber, M., and Srivastava, R. D., J. Chem. Soc. Faraday Trans. I 73, 1692 (1977).
14. Farber, M., and Srivastava, R. D., Chem. Phys. Lett. 51, 307 (1977).
15. Rosenstock, H. M., Draxl, K., Steiner, B. W., and Herron, J. T., "Energetics of Gaseous Ions," J. Phys. Chem. Ref. Data, Vol. 6, 1977 (Supplement No. 1).

Table 1

RELATIVE ION INTENSITIES OF TATB SUBLIMATION
AND THERMAL DECOMPOSITION AT 250 C

	Langmuir Experiments	Effusion Experiments
258	84	
144	7	65
128	20	80
114	7	100
98	25	60
86	7	35
70		60
46		33
44		48
30		30
28		70
18		25
2		4

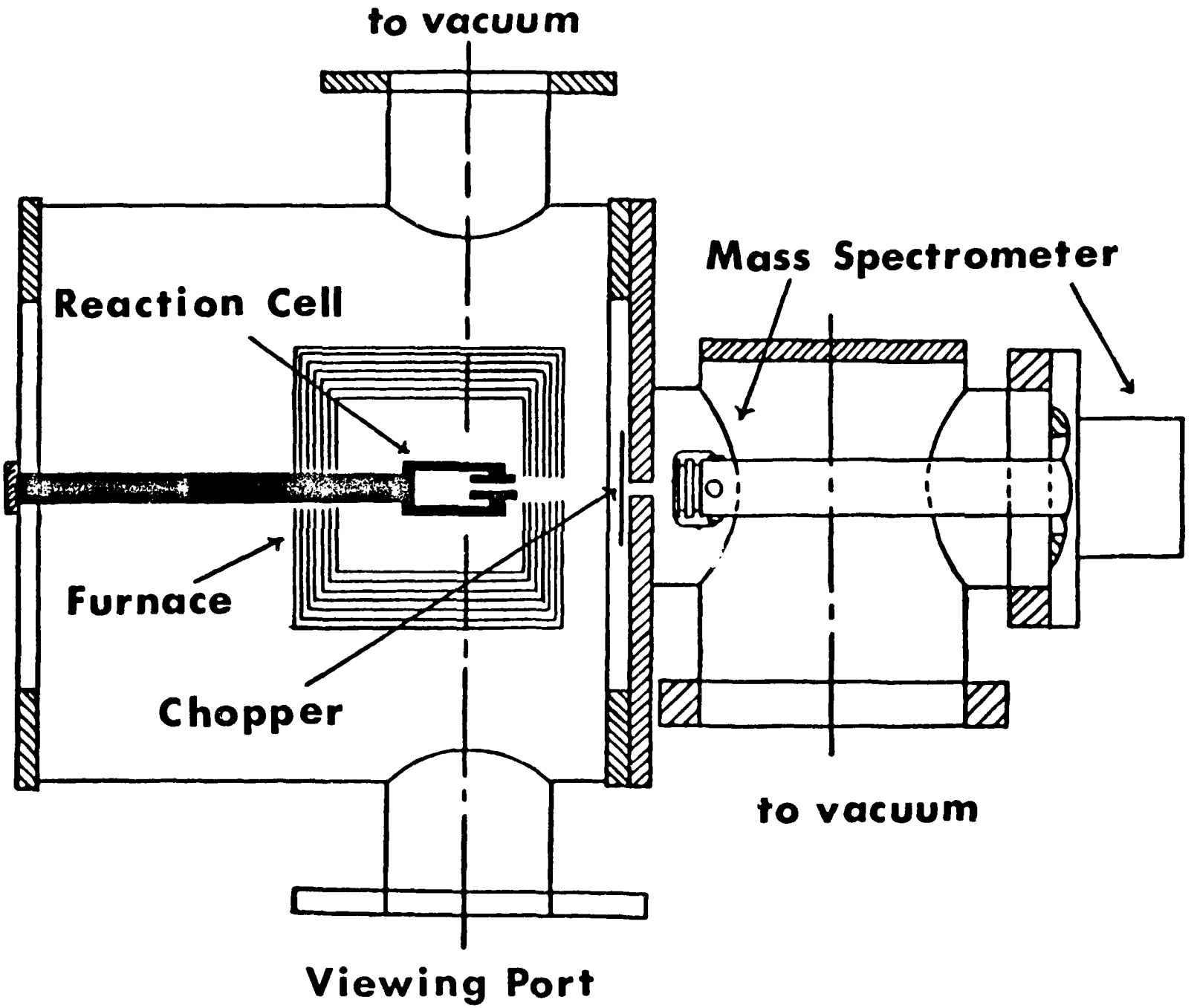

Fig. 1. Dual Vacuum Mass Spectrometer System

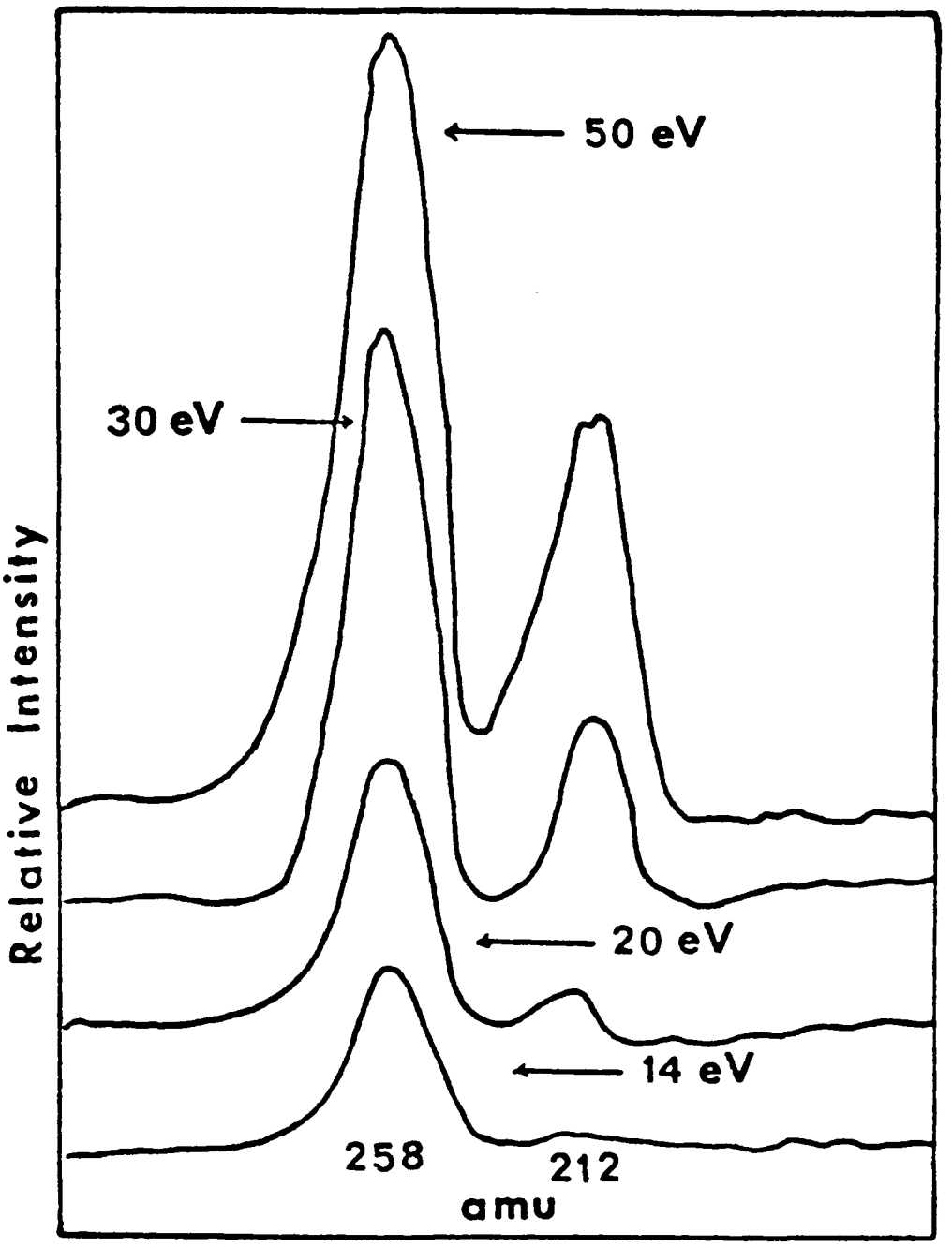

Fig. 2. Electron impact fragmentation pattern of the TATB molecule. The peak at amu 212 is produced within the ionization chamber of the mass spectrometer with varying relative intensities as a function of the ionizing voltage.

Relative Intensity	Ratio (258/212)
50 eV	2
30 eV	3
20 eV	6
14 eV	>100

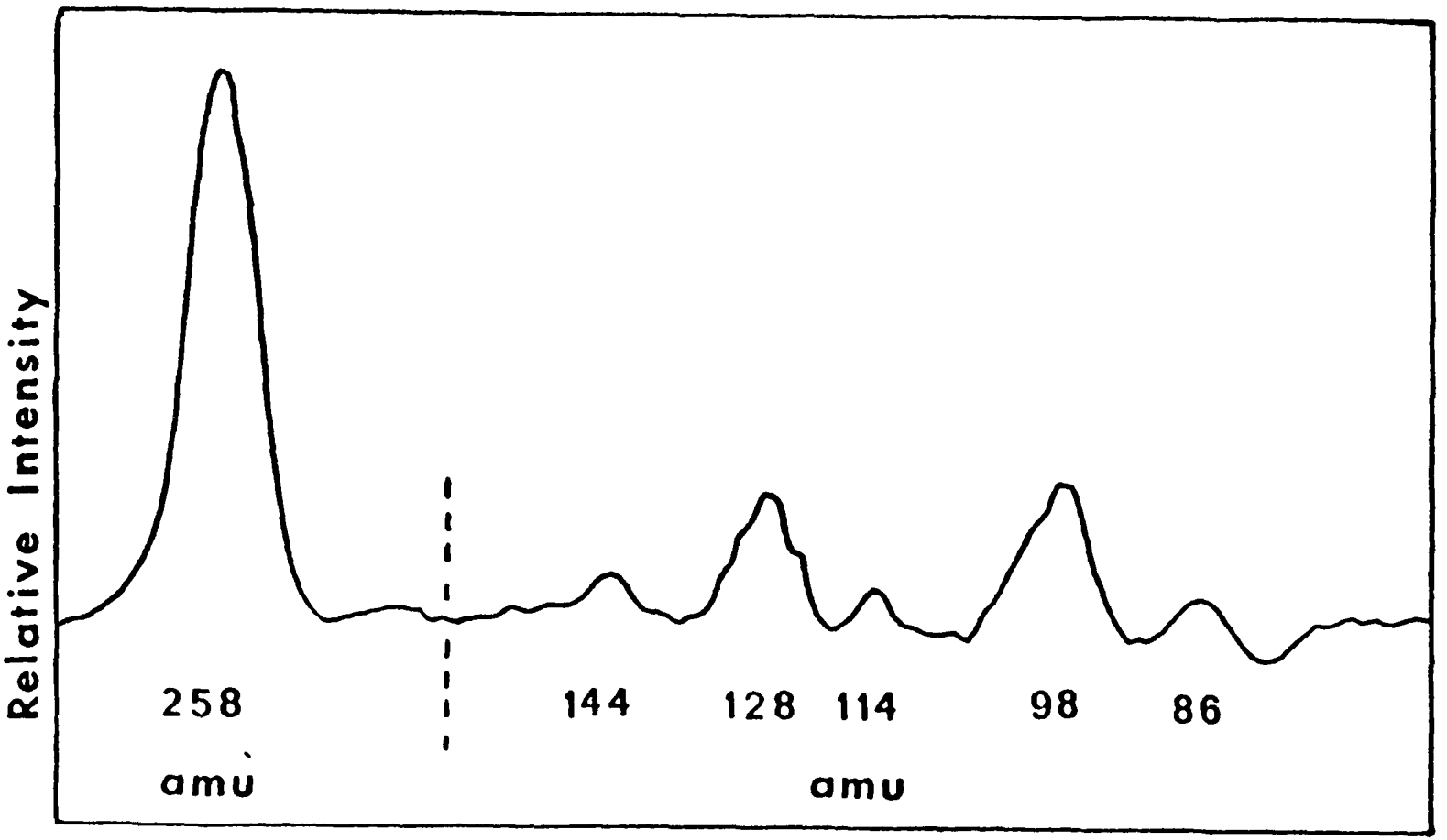

Fig. 3. TATB evaporation and decomposition (Langmuir experiment)

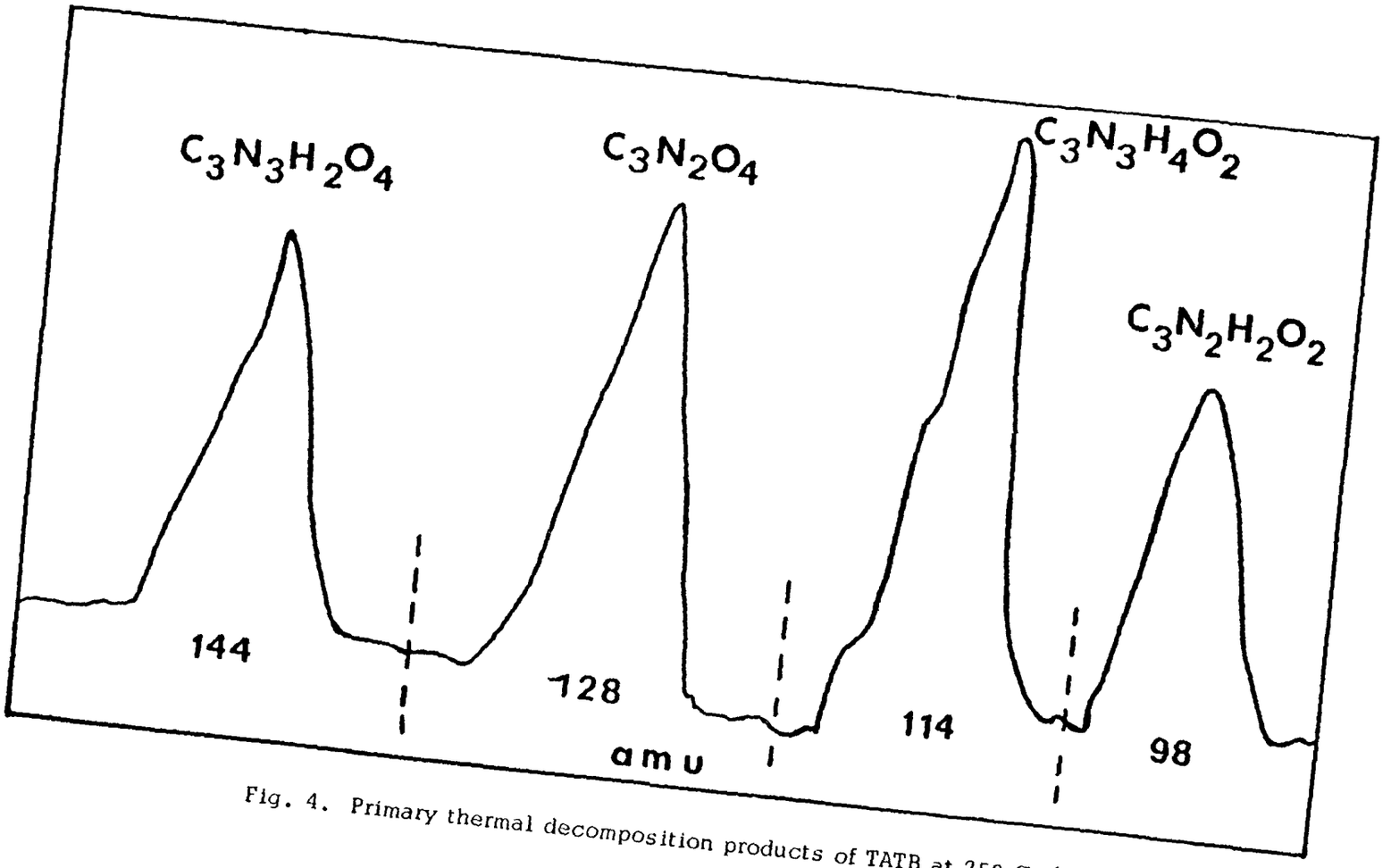

Fig. 4. Primary thermal decomposition products of TATB at 250 C (Effusion Experiment)

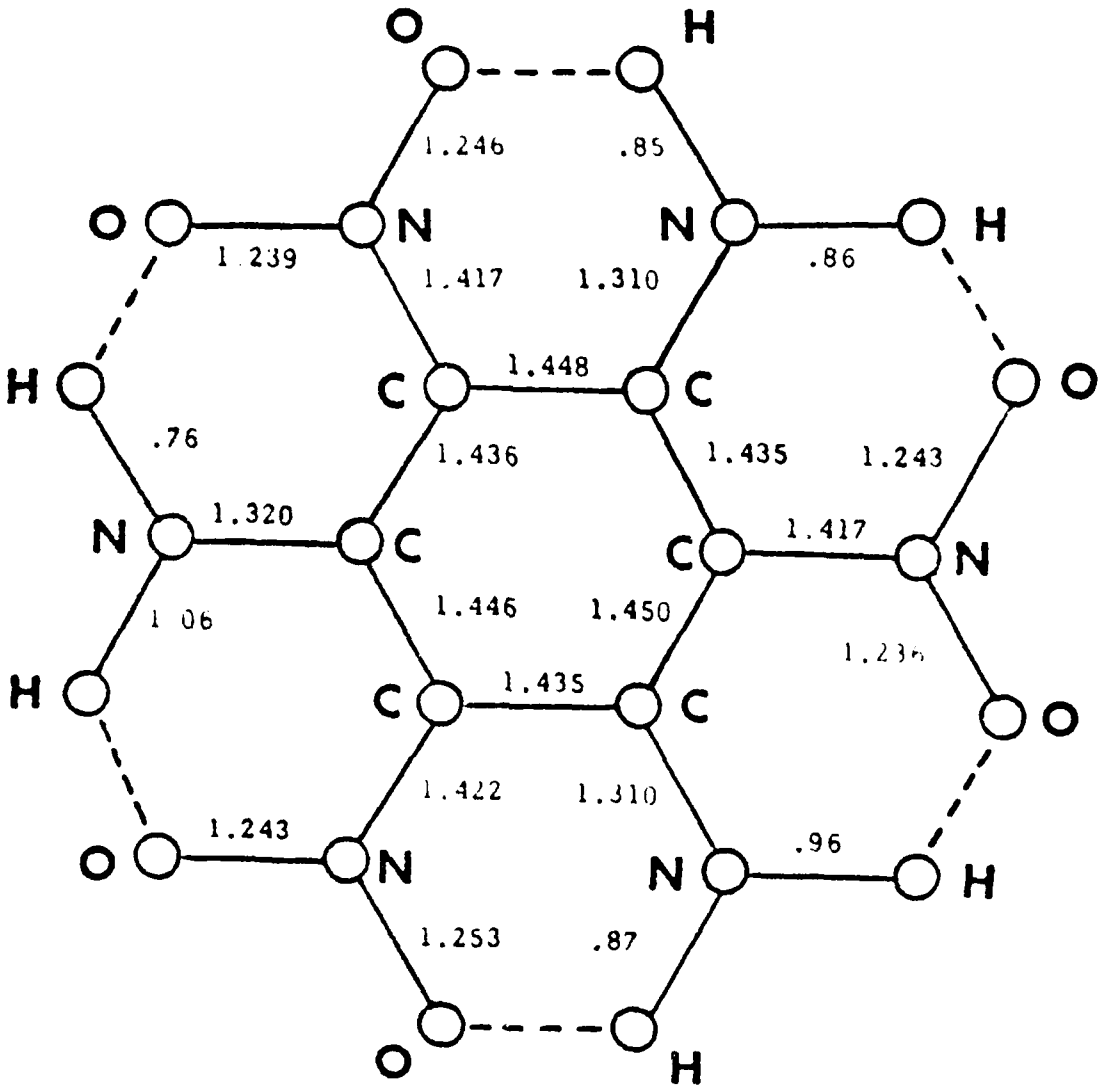

Fig. 5. Bond lengths in Å units from crystallographic experiments of Cady and Larson (2).
Note: Bond lengths are not drawn to scale.

INT.

ENERGETIC MATERIALS RESEARCH

DISTRIBUTION LIST

	No. Copies
Assistant Secretary of the Navy (R, E, and S) Attn: Dr. R.E. Reichenbach Room 5E787 Pentagon Washington, DC 20350	1
Office of Naval Research Code 473 Arlington, VA 22217 Attn: Dr. R. Miller	10
Office of Naval Research Code 200B Arlington, VA 22217 Attn: Dr. J. Enig	1
Office of Naval Research Code 260 Arlingon, VA 22217 Attn: Mr. D. Siegel	1
Office of Naval Research Western Office 1030 East Green Street Pasadena, CA 91106 Attn: Dr. T. Hall	1
Office of Naval Research Eastern Central Regional Office 495 Summer Street Boston, MA 02210 Attn: Dr. L. Peebles Dr. A. Wood	2
Office of Naval Research San Francisco Area Office One Hallidie Plaza Suite 601 San Francisco, CA 94102 Attn: Dr. P. A. Miller	1
Defense Technical Information Center DTIC-DDA-2 Cameron Station Alexandria, VA 22314	12
AFATL Eglin AFB, FL 32542 Attn: Dr. Otto K. Heiney	1
AFRPL Code PACC Edwards AFB, CA 93523 Attn: Mr. W. C. Andrepont	1
AFRPL Code CA Edwards AFB, CA 93523 Attn: Dr. R. R. Weiss	1
Code AFRPL MKPA Edwards AFB, CA 93523 Attn: Mr. R. Geisler	1
Code AFRPL MKPA Edwards AFB, CA 93523 Attn: Dr. F. Roberto	1
AFSC Andrews AFB, Code DLFP Washington, DC 20334 Attn: Mr. Richard Smith	1
Air Force Office of Scientific Research Directorate of Chemical & Atmospheric Sciences Bolling Air Force Base Washington, DC 20332	1
Air Force Office of Scientific Research Directorate of Aerospace Sciences Bolling Air Force Base Washington, DC 20332 Attn: Dr. L. H. Caveny	1
Anal-Syn Lab Inc. P.O. Box 547 Paoli, PA 19301 Attn: Dr. V. J. Keenan	1

	No. Copies
Army Ballistic Research Labs Code DRDAR-BLP Aberdeen Proving Ground, MD 21005 Attn: Mr. L. A. Watermeier	1
Army Ballistic Research Labs ARRADCOM Code DRDAR-BLP Aberdeen Proving Ground, MD 21005 Attn: Dr. Ingo W. May	1
Army Ballistic Research Labs ARRADCOM Code DRDAR-BLT Aberdeen Proving Ground, MD 21005 Attn: Dr. Philip Howe	1
Army Missile Command Code DRSME-RK Redstone Arsenal, AL 35809 Attn: Dr. R. G. Rhoades Dr. W. W. Wharton	2
Atlantic Research Corp. 5390 Cherokee Avenue Alexandria, VA 22314 Attn: Dr. C. B. Henderson	1
Ballistic Missile Defense Advanced Technology Center P.O. Box 1500 Huntsville, AL 35807 Attn: Dr. David C. Sayles	1
Ballistic Research Laboratory USA ARRADCOM DRDAR-BLP Aberdeen Proving Ground, MD 21005 Attn: Dr. A. W. Barrows	1
Hercules Inc. Cumberland Aerospace Division Allegany Ballistics Lab P.O. Box 210 Cumberland, MD 21502 Attn: Dr. Rocco Musso	2
Hercules Inc. Eglin AFATL/DLDL Eglin AFB, FL 32542 Attn: Dr. Ronald L. Simmons	1
Hercules Inc. Magna Bacchus Works P.O. Box 98 Magna, UT 84044 Attn: Mr. E. H. DeButts	1
Hercules Inc. Magna Bacchus Works P.O. Box 98 Magna, UT 84044 Attn: Dr. James H. Thacher	1
HQ US Army Material Development Readiness Command Code DRCDE-DW 5011 Eisenhower Avenue Room 8N42 Alexandria, VA 22333 Attn: Mr. S. R. Matos	1
Johns Hopkins University APL Chemical Propulsion Information Agency Johns Hopkins Road Laurel, MD 20810 Attn: Mr Theodore M. Gilliland	1
Lawrence Livermore Laboratory University of California Livermore, CA 94550 Attn: Dr. M. Finger	1
Lawrence Livermore Laboratory University of California Livermore, CA 94550 Attn: Dr. R. McGuire	1
Lockheed Missiles and Space Co. P.O. Box 504 Sunnyvale, CA 94088 Attn: Dr. Jack Linsk Org. 83-10 Bldg. 154	1

	No. Copies
Lockheed Missile & Space Co. 3251 Hanover Street Palo Alto, CA 94304 Attn: Dr. H. P. Marshall Dept. 52-35	1
Los Alamos Scientific Lab P.O. Box 1663 Los Alamos, NM 87545 Attn: Dr. R. Rogers, WX-2	1
Los Alamos Scientific Lab P.O. Box 1663 Los Alamos, NM 87545 Attn: Dr. B. Craig, M Division	1
Naval Air Systems Command Code 330 Washington, DC 20360 Attn: Mr. R. Heitkotter Mr. R. Brown	1
Naval Air Systems Command Code 310 Washington, DC 20360 Attn: Dr. H. Mueller Dr. H. Rosenwasser	1
Naval Explosive Ordnance Disposal Facility Indian Head, MD 20640 Attn: Lionel Dickinson Code D	1
Naval Ordnance Station Code 5034 Indian Head, MD 20640 Attn: Mr. S. Mitchell	1
Naval Ordnance Station Code PM4 Indian Head, MD 20640 Attn: Mr. C. L. Adams	1
Dean of Research Naval Postgraduate School Monterey, CA 93940 Attn: Dr. William Tolles	1
Naval Research Lab Code 6510 Washington, DC 20375 Attn: Dr. J. Schnur	1
Naval Research Lab Code 6100 Washington, DC 20375	1
Naval Sea Systems Command Washington, DC 20362 Attn: Mr. G. Edwards, Code 62R3 Mr. J. Murrin, Code 62R2 Mr. W. Blaine, Code 62R	1
Naval Sea Systems Command Washington, DC 20362 Attn: Mr. R. Beauregard SEA 64E	1
Naval Surface Weapons Center Code R11 White Oak, Silver Spring, MD 20910 Attn: Dr. H. G. Adolph	1
Naval Surface Weapons Center Code R13 White Oak, Silver Spring, MD 20910 Attn: Dr. R. Bernecker	1
Naval Surface Weapons Center Code R10 White Oak, Silver Spring, MD 20910 Attn: Dr. S. J. Jacobs	1
Naval Surface Weapons Center Code R11 White Oak, Silver Spring, MD 20910 Attn: Dr. M. J. Kamlet	1
Naval Surface Weapons Center Code R04 White Oak, Silver Spring, MD 20910 Attn: Dr. D. J. Pastine	1
Naval Surface Weapons Center Code R13 White Oak, Silver Spring, MD 20910 Attn: Dr. E. Zimet	1

	No. Copies
Naval Surface Weapons Center Code R101 Indian Head, MD 20640 Attn: Mr. G. L. MacKenzie	1
Naval Surface Weapons Center Code R17 Indian Head, MD 20640 Attn: Dr. H. Haiss	1
Naval Surface Weapons Center Code R11 White Oak, Silver Spring, MD 20910 Attn: Dr. K. F. Mueller	1
Naval Surface Weapons Center Code R16 Indian Head, MD 20640 Attn: Dr. T. D. Austin	1
Naval Surface Weapons Center Code R122 White Oak, Silver Spring, MD 20910 Attn: Mr. L. Roslund	1
Naval Surface Weapons Center Code R121 White Oak, Silver Spring, MD 20910 Attn: Mr. M. Stosz	1
Naval Weapons Center Code 3853 China Lake, CA 93555 Attn: Dr. R. Atkins	1
Naval Weapons Center Code 3205 China Lake, CA 93555 Attn: Dr. L. Smith	1
Naval Weapons Center Code 3205 China Lake, CA 93555 Attn: Dr. C. Thelen	1
Naval Weapons Center Code 385 China Lake, CA 93555 Attn: Dr. A. Amster	1
Naval Weapons Center Code 388 China Lake, CA 93555 Attn: D. R. Derr	1
Naval Weapons Center Code 388 China Lake, CA 93555 Attn: Dr. R. Reed Jr.	1
Naval Weapons Center Code 385 China Lake, CA 93555 Attn: Dr. A. Nielsen	1
Naval Weapons Center Code 3858 China Lake, CA 93555 Attn: Mr. E. Martin	1
Naval Weapons Center China Lake, CA 93555 Attn: Mr. R. McCarten	1
Naval Weapons Support Center Code 5042 Crane, Indiana 47522 Attn: Dr. B. Douda	1
Rohm and Haas Company 723-A Arcadia Circle Hunsville, Alabama 35801 Attn: Dr. H. Shuey	1
Strategic Systems Project Office Dept. of the Navy Room 901 Washington, DC 20376 Attn: Dr. J. F. Kincaid	1
Strategic Systems Project Office Dept. of the Navy Room 1048 Washington, DC 20376 Attn: Mr. E. L. Throckmorton Mr. R. Kinert	2
Thiokol Chemical Corp. Brigham City Wasatch Division Brigham City, UT 84302 Attn: Dr. G. Thompson	1

	No. Copies
USA ARRADCOM DRDAR-LCE Dover, NJ 07801 Attn: Dr. R. F. Walker	1
USA ARRADCOM DRDAR-LCE Dover, NJ 07801 Attn: Dr. N. Slagg	1
U.S. Army Research Office Chemistry Division P.O. Box 12211 Research Triangle Park, NC 27709	1
Washington State University Dept. of Physics Pullman, WA 99163 Attn: Professor G.D. Duval	1
Space Sciences, Inc. 135 West Maple Avenue Monrovia, CA 91016 Attn: Dr. M. Farber	1
SRI International 333 Ravenswood Avenue Menlo Park, CA 94025 Attn: Mr. M. Hill	1
Office of Naval Research Code 421 Arlington, VA 22217 Attn: Dr. B. Junker	1
The Johns Hopkins University Department of Chemistry Balitmore, MD 21218 Attn: Dr. Joyce J. Kaufman	1
University of California Department of Chemistry Berkeley, CA 94720 Attn: Professor Y.T. Lee	1
Office of Naval Research Code 472 Arlington, VA 22217 Attn: Dr. G. Neece	1
University of California Department of Chemistry 405 Hilgard Avenue Los Angeles, CA 90024 Attn: Professor M. Nicol	1
University of California Energy Center Mail Code B-010 La Jolla, CA 92093 Attn: Prof. S.S. Penner	1
University of Washington Department of Chemistry Seattle, Washington 98195 Attn: Prof. B.S. Rabinovitch	1
Dr. P. Rentzepis Bell Laboratories Murrary Hill N.J. 07971	1
University of Southern CA Department of Electrical Engineering University Park Los Angeles, CA 90007 Attn: C. Wittig	1
MIT Dept. of Chemistry Cambridge, MA 02139 Attn: Prof. John Deutsch	

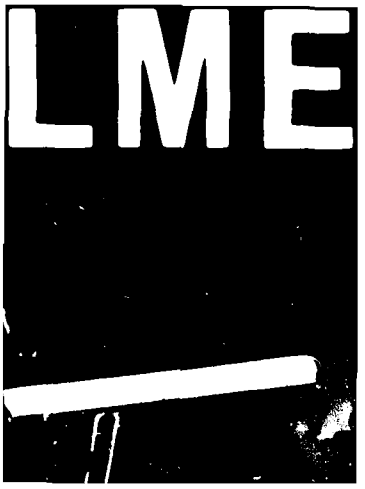
LME